



Norwegian University of
Science and Technology

A Study of Deep Sea Mining Electrical Power System Topologies

Fredrik Sigmund Qvigstad Williksen

Master of Energy and Environmental Engineering

Submission date: June 2017

Supervisor: Elisabetta Tedeschi, IEL

Co-supervisor: Razieh Fard, IEL

Norwegian University of Science and Technology
Department of Electric Power Engineering

Preface

This report is the final product of my Masters Degree at the Department of Electric Power Engineering at the Norwegian University of Science and Technology. This thesis corresponds to a workload of 30 ECTS.

The writing of this thesis has been interesting and motivating, but also annoying, frustrating and seemingly hopeless at certain times. Despite this, working with this thesis has given me valuable experience of finding, investigating, evaluating, processing and presenting information and data that have been the groundwork of several hours of work.

I would like to express my greatest gratitude to my co-supervisor PhD Candidate Razieh Nejati Fard for valuable guidance, and help with the simulation software. I would also like to thank my supervisor, Professor Elisabetta Tedechi, for giving me great freedom to focus the thesis towards my own preferences.

I would also like to thank Ane Dideriksen for assistance with proof-reading in the finishing stages of the work with this thesis.

Trondheim 28.06.2017
Fredrik Sigmund Qvigstad Williksen

Summary

Deep sea mining (DSM) is an emerging technology. The ever-increasing world-wide need for minerals in growing markets and industries of developing countries has made DSM financially reasonable. As there are few known system concepts for DSM it is important to investigate the different possibilities of system design and operation of the future DSM production systems. This thesis has, by investigating R&D and system concepts that are under development, presented different solutions for the electrical distribution system of a DSM production system capable of operating in the Norwegian Sea.

In this thesis it is assumed that the DSM production system will consist of three subsea mining machines (referred to as seafloor production tools (SPTs)) designed to excavate, process and collect ore at the seafloor. The electrical power system is estimated to operate at depths up to 3,500 m, where the production system will mine seafloor massive sulfide deposits formed through hydrothermal activity. A positive displacement pump, powered by pressurized seawater from the topside installation, is used for all the proposed system topologies.

Firstly, simplified models were made in order to investigate three different system topologies of powering the SPTs. In the first model the different components of the SPTs were to be powered individually, thus reducing the number of subsea components by placing the frequency converter of the components at the TS. The simulation proved that powering the SPT components individually would result in excessive power losses, thus ruling out this system topology. In addition the machines of the SPTs perform better when the converters are installed on board the SPTs. Two other system topologies were proposed. The first is powering each of the three SPTs individually from the topside installation. The second is having a combined power distribution to a subsea distribution station which distributes the power to the SPTs. Both these system topologies were deemed suitable for powering a DSM system. Therefore, four simulation models were made in order to investigate the possibilities of power distribution to a DSM production system. The simulation software PowerFactory is used. Two models utilize AC distribution to the subsea components of the production system, and the two other models use DC distribution. The AC models have a distribution voltage of 6.6 kV operating at 60 Hz and the DC models operate at ± 3 kV. The voltage levels are chosen in order to obtain a realistic comparison between the two.

The simulations performed in this thesis prove that the distribution losses will be lower when powering the subsea mining machines through a subsea distribution station compared to the individual power distribution. In addition will the losses be even lower if DC distribution is utilized. By reducing the power losses the production system will be less expensive to operate due to lower fuel consumption. Harmonic content will also be an issue for the proposed AC system topologies, and

measures should be done in order to reduce the influence of such power quality pollution.

Although the combined distribution to a subsea station will have the lowest power loss, this system will have a large investment cost as the number of subsea components are increased. Advanced analysis will therefore be necessary to evaluate which system topology should be used for powering a DSM power system. However, due to the large power requirement of possible DSM in the Norwegian Sea, a combined distribution to a subsea distribution station will most likely be recommended for DSM operations in the Norwegian Sea.

Sammendrag

Dyphavsgruvedrift (eng. Deep sea mining - DSM) er en fremtredende industri. Den verdensomspennende økende etterspørselen etter mineraler i markeder og industrer i blant annet utviklingsland har gjort DSM økonomisk fornuftig. Siden det er få kjente systemer for DSM er det viktig å undersøke forskjellige muligheter for utformingen og driften av slike produksjonssystemer. Denne oppgaven vil, ved å undersøke forskning innenfor området, presentere fire forskjellige elektriske kraftsystem som kan drifte et DSM produksjonssystem.

I denne oppgaven er det antatt at et DSM produksjonssystem vil bestå av tre maskiner som er spesialdesignet for å arbeide med mineralutvinning på havbunnen. Maskinene er kalt Seafloor Production Tools - SPTs på engelsk. The elektriske kraftsystemet vil bli designet for å bli driftet på 3500 meters dyp. Der vil SPTene drive gruvedrift i områdene rundt hydrotermale skorsteiner. I alle de foresatte modellene er en fortrenningspumpe brukt for å frakte mineralene til overflateinstallasjonen.

Først ble forenklede modeller laget for å undersøke mulige distribusjonsalternativ til SPTene. I den første modellen er hver komponent på SPTen utstyrt med en egen kraftforsyning slik at frekvensomformerne til motorene kan plasseres på overflateskipet. Simuleringene viste at distribusjonstapene ble veldig store, og denne modellen ble utelukket. I tillegg til de store tapene vil motorene virke bedre med frekvensomformerne plassert på SPTene. De to andre foreslåtte modellene vil distribuere kraften til hver SPT for seg og den siste foreslår å ha en undersjøisk distribusjonsstasjon som vidrefordeler elektrisk energi til SPTene. Begge disse systeme ble anslått å være passende for å drive et DSM produksjonssystem, og fire modeller ble laget basert på de forenklede modellene: to med 60 Hz vekselspanning (6,6 kV) og to med likespenning (± 3 kV). Simuleringsverktøyet PowerFactory er brukt. Spenningsnivåene er valgt for å gi en realistisk sammeligning mellom de to typene (AC vs DC).

Simuleringene i denne oppgaven viser at distribusjonstapene er lavest for systemene som leverer elektrisk kraft til en undersjøisk distribusjonsstasjon. Tapene vil bli enda lavere dersom likespenning blir brukt isteden for vekselspanning. Lave distribusjonstap vil gi lavere driftstap ettersom mindre drivstoff vil bli brukt. Dersom vekselspanning blir brukt vil komponentene tilføre harmonisk forurensning til systemet og tiltak må gjøres for å begrense dette.

Selv om systemene som leverer elektrisk kraft til en undersjøisk distribusjonsstasjon har det laveste krafttapet vil systemet ha en høy produksjonskostnad grunnet den undersjøiske distribusjonsstasjonen. Avanserte analyser vil være nødvendig for å evaluere hvilket system som burde brukes til å drifte et DSM produksjonssystem. Uansett, grunnet et høyt kraftbehov for mulig gruvedrift i Norskehavet vil systemet med en undersjøisk distribusjonsstasjon bli anbefalt for dypvannsgruvedrift i Norskehavet.

Contents

Preface	i
Summary	ii
Sammendrag	iv
Contents	v
List of Figures	viii
List of Tables	ix
Nomenclature	xi
1 Introduction	1
1.1 Objective	1
1.2 Method	1
1.3 Scope	2
1.4 Citations from other Papers	2
1.5 Structure of the Report	3
2 Background	4
2.1 Motivation for Deep Sea Mining	4
2.1.1 Seafloor Mineral Deposits	4
2.1.2 Mining Sites Within Norwegian Jurisdiction	5
2.2 Deep Sea Mining System Topologies	6
2.2.1 Nautilus Minerals Solwara 1 Project	6
2.2.2 BAUER and Technip Vertical Miner	7
2.3 Deep Sea Mining System Components	9
2.3.1 Seabed System	9
2.3.2 Underwater Transportation System	10
2.3.3 Topside System	12
3 Theory	14
3.1 Power Quality in Offshore Grids	14
3.1.1 Harmonic Content	16
3.1.2 Power Factor	20
3.2 Reactive Power Compensation and Harmonic Content Reduction . .	21
3.2.1 SVC and STATCOM	21

3.2.2	Control of APF	24
3.3	Cables	25
4	Deep Sea Mining Power System Topologies and Modelling	28
4.1	Power Estimation for DSM Operations in the Norwegian Sea	28
4.1.1	SS	29
4.1.2	UTS	29
4.1.3	TS	29
4.2	Different System Topology Configurations	31
4.2.1	Simplified Models	31
4.2.2	Model 1: Individual 60 Hz AC Distribution	32
4.2.3	Model 2: Combined 60 Hz AC Distribution	33
4.2.4	Model 3: Individual DC Distribution	34
4.2.5	Model 4: Combined DC Distribution	35
4.2.6	Modelling of SPT Components	36
4.2.7	Modelling of TS and UTS	37
5	Simulations and Results	38
5.1	Simple Models	38
5.1.1	Model A and B Load Flow Analysis	38
5.1.2	Motor Start Up Analysis	39
5.1.3	Model C Load Flow Analysis	42
5.1.4	Simple Model Simulations Summary	43
5.2	Steady State Load Flow Analysis	44
5.2.1	Model 1 and Model 2	45
5.2.2	Model 3 and Model 4	46
5.3	Harmonics and Power Quality Analysis	48
5.3.1	Model 1	49
5.3.2	Model 2	49
5.3.3	Model 3 and Model 4	50
5.4	BC Mining Tool Motor Start Up	51
5.4.1	Motor Buses During Start Up	51
5.4.2	Influence on Other Buses	52
6	Discussion	54
6.1	Simple Models	54
6.2	Model Structure and Cost Comparison	55
6.2.1	Individual SPT Power Distribution (Model 1 and Model 3)	55
6.2.2	Combined Subsea Power Distribution (Model 2 And Model 4)	56
6.2.3	Converters	57
6.3	AC Distribution	58
6.4	DC Distribution	60
6.5	Reducing Harmonics	61
6.6	Voltage Fluctuations	62
7	Conclusion	63

References	65
Appendices	69
A Growth stages of SMS deposits	69
B Estimation of SPT installed pump effect	70
C DSM System Topologies	72
C.1 Nautilus Minerals' SPS	72
C.2 BAUER and Technip Vertical Miner	73
D Single Line Diagrams	74
D.1 Symbols	74
D.2 Simple Models	75
E Model A, B and C Load Flow Simulation Results	77
F Model 1, 2, 3 and 4 Load Flow Simulation Results	81
G Cable Data	83

List of Figures

2.1	Illustration of vertical trench cutting method.	7
2.2	Sketch of the vertical cutter developed by BAUER and Technip.	8
3.1	Utility source, power electronic load and other loads connected to a PCC.	16
3.2	Distorted line current made up of fundamental current and distorted harmonic pollution.	17
3.3	Circuit equivalent of TCR and TSCs, both shunt connected	22
3.4	V-Q characteristics of the SVC and the STATCOM.	23
3.5	STATCOM with a Current-Mode Controller.	24
3.6	The nominal π -equivalent circuit of a medium length transmission line.	25
3.7	Illustration of the cable limitation in active power transfer due to reactive charging current.	27
4.1	Model 1 SLD.	32
4.2	Model 2 SLD.	33
4.3	Model 3 SLD.	34
4.4	Model 4 SLD.	35
5.1	Model D: Motor bus voltage and motor speed during start up.	40
5.2	Active and reactive power consumption during star up for both converter configurations in Model D.	41
5.3	Harmonic current injected in relation to fundamental current I_h/I_1	48
5.4	Motor bus voltage during start up of the BC mining tool.	52
5.5	Bus voltages during start up of the BC mining tool.	53
A.1	Schematic diagram showing hypothesis for the development of SMS mounds on the seafloor	69
C.1	Nautilus Minerals' SPS	72
C.2	BAUER and Technip Vertical Miner	73
D.1	Model A, B and C SLD.	75
D.2	Model D SLD.	76
E.1	Load Flow Model A.	78
E.2	Load Flow Model B.	79
E.3	Load Flow Model C.	80

List of Tables

2.1	Estimated share of total installed power for the Solwara 1 SPT components.	10
2.2	Installed power of DSM system components.	13
3.1	Allowed harmonic current distortion.	19
4.1	Installed power of the DSM system components designed for operation at 3,500 m depth.	30
4.2	The motor type chosen for the different SPT components and SSLP pump drive.	36
5.1	Power loss in Model A and B.	38
5.2	Technical parameters of the motor in Model D.	39
5.3	Summary of Model D motor start up simulation.	39
5.4	Model C load flow simulation cable size, loading and voltage drop.	42
5.5	Loading of SPT- and TS-components during steady state load flow analysis Model 1-4.	44
5.6	Model 1: Load flow simulation cable size, loading, voltage drop, current and power loss.	45
5.7	Model 2: Load flow simulation cable size, loading, voltage drop, current and power loss.	46
5.8	Model 3: Load flow simulation cable size, loading, voltage drop, current and power loss.	46
5.9	Model 4: Load flow simulation cable size, loading, voltage drop, current and power loss.	47
5.10	THD and I_{SC} for all AC buses in Model 1.	49
5.11	THD and I_{SC} for topside and subsea AC buses in Model 2.	50
5.12	THD and I_{SC} for the topside AC bus (PSV) in Model 3 and Model 4.	50
5.13	Summary of BC mining tool motor start up.	51
6.1	Converter requirement for all models.	57
6.2	P_{SIL} of the cables selected for AC distribution.	58
6.3	Harmonic currents absorbed by the filter.	61
D.1	Explanation of SLD Symbols.	74
E.1	Model A and Model B load flow simulation cable size, loading and voltage drop.	77

F.1	Model 1 and 2: Load flow simulation results.	81
F.2	Model 3 and 4: Load flow simulation results.	82
G.1	Technical data of the cables selected for AC distribution.	83
G.2	Technical data of the cables selected for DC distribution.	83

Nomenclature

Abbreviations

AC	Alternating Current
AMOR	Arctic Mid-Ocean Ridge
APF	Active Power Filter
DC	Direct Current
DP	Dynamic Positioning
DP	Dynamic Positioning
DPF	Displacement Power Factor
DSM	Deep Sea Mining
EMI	Electromagnetic Interference
HPU	Hydraulic Power Unit
HV	High Voltage
LARS	Launch and Recovery System
MV	Medium Voltage
O&G	Oil and Gas
PCC	Point of Common Coupling
PD	Positive Displacement
PDP	Positive Displacement Pump
PF	Power Factor
PSV	Production Support Vessel
R&D	Research and Development
RALS	Riser and Lifting System
RMS	Root Mean Square
SDS	Subsea Distribution Station
SIL	Surge Impedance Loading
SLD	Single-line diagram

SMS	Seafloor Massive Sulfide
SPS	Seafloor Production System
SPT	Seafloor Production Tool
SS	Seabed System
SSLP	Subsea Slurry Lift Pump
SVC	Static VAR Compensator
TCR	Thyristor Controlled Reactor
THD	Total Harmonic Distortion
TS	Topside System
TSC	thyristor-switched capacitors
UTS	Underwater Transportation System
XLPE	Cross(X)-Linked Polyethylene

Metric Prefix

μ	micro	10^{-6}
k	kilo	10^3
M	mega	10^6
m	milli	10^{-3}

Symbols

ω	angular frequency	rad/s
B	cable shunt susceptance	S
C	cable shunt capacitance per phase per unit length	F/km
f	frequency	Hz
f_1	fundamental frequency	Hz
f_h	harmonic frequency at the h harmonic	Hz
G	cable shunt conductance	S
g	cable shunt conductance per phase per unit length	S/km
i_1	fundamental source current	A
I_h	RMS harmonic current at harmonic h	A
i_h	harmonic current component at the h harmonic frequency	A
I_P	active current	A

I_Q	reactive current	A
i_s	source current	A
i_{s1}	fundamental source current	A
I_{SC}	short-circuit fault current	A
I_{TL}	maximum current at the thermal limit	A
j	imaginary unit or unit imaginary number	[-]
L	per-phase cable inductance per unit length	H
l	cable length	km
L_s	internal source impedance	H
P	active power	W
P_R	Power at receiving end	W
P_{SIL}	delivered power at SIL	W
Q_{cons}	consumed reactive power	VAr
Q_{prod}	produced reactive power	VAr
R	per-phase cable resistance	Ω
r	per-phase cable resistance per unit length	Ω
S	apparent power	VA
U_n	nominal (line-to-line) RMS voltage	V
V_d	voltage drop	V
V_h	RMS harmonic voltage at harmonic h	V
V_n	nominal voltage of cable, line-to-line	V
V_s	RMS source voltage	V
v_s	source voltage	V
V_{LL}	line-to-line voltage	V
X	per-phase cable reactance	H
Y	total cable shunt admittance	S
Z	total cable series impedance	Ω
Z_c	characteristic impedance	Ω

Units

Ω	ohm	
I_s	source current RSM value	A

A	ampere
F	farad
H	henry
h	hour
hp	horsepower
Hz	hertz
m	meter
rad/s	radians per second
S	siemens
t	Tonne
V	volt
VA	volt-ampere
VAr	volt-ampere reactive
W	Watt

Chapter 1

Introduction

1.1 Objective

The objective of this master thesis will be to investigate different electrical power system topologies for deep sea mining (DSM) application in the Norwegian Sea. Both existing and possible DSM production system topologies will be presented and their electrical power systems will be investigated and simulated using the simulation tool DlgSILENT©PowerFactory. The different components of existing DSM technology will be presented and their representation in the simulation tool will be explained.

In order to compare the different system topologies to one another the same simulations will be done for all models. The results of the simulations will be discussed and form the basis of an evaluation of the different topologies suitability for DSM operations. This thesis will attempt to suggest a system topology of the electrical power system for DSM application in the Norwegian Sea. The thesis will aim to illustrate the influence the physical structure of a electrical power system topology will have for DSM application.

1.2 Method

A preliminary study ([1]) of electrical power systems for DSM application have been carried out ahead of this thesis. The study includes a literature review of DSM technology and a simulation model was developed in the simulation software PowerFactory. This simulation model has been further developed during the work of this thesis.

As in the preliminary study this thesis will include a minor literature review. This is due to the fact that the preliminary study solely focused on the production system developed by Nautilus Minerals. The literature review will study other solutions for the different parts of a DSM production system by reviewing different conference papers and research done by companies delivering solutions to DSM system developers.

To understand the measures needed to obtain a functional electric power system for DSM relevant theory will be studied. Electric *power quality* will be in focus and different aspects of maintaining it.

The investigated literature, papers and information will be presented and form

the basis of the development of the simulation models. The components of the simulation models will be controlled by comparison to industrial equipment of similar rating and applications as DSM.

Trough simulations the thesis will discuss and conclude which electrical power system topology will be most proper for powering a DSM production system in the Norwegian Sea.

1.3 Scope

The scope of this thesis will be to investigate the system topologies of existing DSM production systems and the required power the different components of a deep sea mining production system require. Available scientific contributions and information on existing system topologies will be studied. Relevant theory is to be presented, but electrical components of offshore power systems will not be described in detail as it is assumed that the reader will have general knowledge of electrical power system components.

The scope of the simulations in this thesis is to provide results that verifies the concluding remarks regarding the design of an electrical power system for DSM application. The simulation models will not focus on the design of the topside installation/vessel of a DSM system. The subsea components of the DSM system will be modelled as accurate as necessary in order to differentiate the behaviour of the simulated system topologies. The simulation software DlgSILENT©PowerFactory is to be used.

All environmental, political and advanced economical aspects of deep sea mining applications are beyond the scope of this thesis.

1.4 Citations from other Papers

Some parts of this thesis are cited from other papers. If a section or part of a sentence is cited, it will be clearly stated. Citations in sentences are marked with quotation marks and written in italics, like this [reference number]: "*Lorem ipsumdolor sit amet, consectetur adipiscing elit.*". If an entire section or chapter is cited the text will be marked with indentation, like this [reference number]:

Lorem ipsum dolor sit amet, consectetur adipiscing elit. Ut purus elit, vestibulum ut, placerat ac, adipiscing vitae, felis. Curabitur dictum gravida mauris. Namarcu libero, nonummy eget, consectetur id, vulputate a, magna. Donec vehicula augue eu neque.

All the references within a citation will correspond to the reference list of this thesis, not the reference list of the cited reference.

1.5 Structure of the Report

Chapter 2 contains a short introduction to motivation for deep sea mining. The different investigated system topologies and system components of DSM production systems are presented.

Chapter 3 is the theory-chapter of the thesis, focusing on power quality in offshore power systems and relevant components.

Chapter 4 presents the power estimation of DSM operations in the Norwegian Sea. The proposed system topology configurations are also presented in this chapter. The PowerFactory representation of the DSM electric system components is also presented.

Chapter 5 presents the simulations of the PowerFactory models and the results of the simulations. Steady state load flow analysis, power quality simulations and motor start up simulations are performed.

Chapter 6 Discusses the proposed system topologies and the results of the simulations.

Chapter 7 is the report conclusion. Suggestion for further work is included.

Chapter 2

Background

This chapter aims to explain the motivation of developing offshore mining systems and to present existing system topologies for DSM operations. A majority of the information in this chapter is based on [1], a preliminary study to this thesis.

2.1 Motivation for Deep Sea Mining

DSM has been an element of discussion in academia and industry since the 1970s, with several pilot mining tests during the 1980s. These projects, using technology from the O&G industry, was triggered by interest of manganese nodules located at depths beyond 5,000m below sea level. Due to low prices for metal, combined with improved technology for land-based mining, the development within deep sea mining ceased due to lack of economic interest. However, research and development continued through the 1990s and 2000s. Today, one of the primary drivers of taking the mining industry offshore is the continuous worldwide economic growth. Emerging markets in developing countries affects the demand of minerals as development of new technology, e.g. within energy applications, increase the demand. Another aspect of the transition to offshore mining is the reduced environmental impact, compared to land based mining. Onshore, declining metal grades results in increased mining waste and a larger environmental footprint as larger areas are processed in order to meet the worldwide demand of metals. These trends in the mining industry will make DSM financially reasonable [1].

2.1.1 Seafloor Mineral Deposits

There are three types of marine mineral deposits of economical interest: Seafloor massive sulfides (SMS), Polymetallic nodules and Cobalt-rich ferromanganese crusts [2].

SMS are (primarily) located along mid-ocean ridges, but also on submarine volcanic arcs. SMS are known to contain large amounts of high grade copper, lead and zinc and some gold and silver [3]. SMS deposits along mid-ocean ridges are made by so-called hydrothermal vents. Reference [4] states: "*SMS deposits form through hydrothermal activity; cold seawater percolates down through the seafloor, is heated through geothermal energy, becomes buoyant and rises, dissolving metals and sulfides from the surrounding rocks*". As this mineral-rich fluid reaches the seafloor a 'smoker' is established where the fluid is cooled and forms a chimney shaped mineral sulfide mound. Both active and inactive hydrothermal vents are referred

to as SMS deposits that can be exploited in marine mining operations. SMS are usually located at depths between 1,400-3,700 m [2]. The process of the formation of a SMS deposit is depicted in Appendix A.

2.1.2 Mining Sites Within Norwegian Jurisdiction

The Arctic Mid-Ocean Ridge (AMOR) stretches along the Norwegian continental shelf between 71°N to 79°N. A well known active hydrothermal vent site named Loki's Castle (73°30'N, 8°E) is located along the AMOR and lies within Norwegian Jurisdiction [5]. Loki's Castle lies at a depth of 2,400 m [2] and contains five active smokers venting smoker fluid of 310-320°C. Two 20-30 m high sulphide mounds have developed around the venting areas, each mound around 150–200 m wide [5]. Loki's Castle has a large potential as a SMS mining site as 51,100 t copper, 55,600 t zinc, 1.72 t gold, and 86 t silver are found to be recoverable according to combined geotechnical and economic analysis presented in [2].

As Loki's Castle is located 540 km from shore the DSM system cannot be connected to the utility grid of Norway. Therefore, a DSM production system with on board diesel-generators for power production is necessary.

2.2 Deep Sea Mining System Topologies

Reference [6] divides DSM systems into three different parts: Seabed Systems (SS), Underwater Transportation System (UTS) and Topside System (TS). The SS consists of one or more subsea machines designed to excavate the mineral-rich seafloor. The machines prepares the ore for the UTS, which transports the ore to the surface as a mixture of ore and seawater, referred to as a slurry. The UTS is driven by one or several pumps, located either topside, subsea or in intervals along the UTS riser pipe. The TS is placed on a production vessel. Once the slurry is brought to the TS it is dewatered and the ore is stored and later transported to shore facilities for further processing. Having the TS on a vessel makes the DSM system very mobile, which is required as the system will operate over large areas.

2.2.1 Nautilus Minerals Solwara 1 Project

Reference [1] presents the Seafloor Production System (SPS) developed by Nautilus Minerals which is to be used in the Solwara 1 Project. This system is the first full scale deep sea mining system, scheduled to start production during 2018. The Solwara 1 project will mine a SMS deposit in the coastal waters of Papa New Guinea (the Bismarck Sea) at a depth of approximately 1,600 m.

The SS in this SPS consist of three Seafloor Production Tools (SPT) designed to cut, process and collect the seabed cuttings. The SPTs are designed by combining mining- and subsea technology. Each SPT has its own umbilical from the TS to provide power, communication and control.

The Solwara 1 UTS consist of a 3-pipe rigid steel riser and a subsea slurry lift pump (SSLP), and is referred to as the Riser and Lifting System (RALS). The SSLP is located subsea, at the end of the steel riser, and it is powered by pressurized seawater from the TS.

The TS is located on board a Production Support Vessel (PSV) equipped with a dynamic positioning (DP) system. The PSV is the operational base of the entire SPS, and it contains power generation, control centers, ore dewatering and storage, launch and recovery systems (LARS) for the SPTs and storage and handling systems for the UTS steel riser. The Nautilus Minerals Solwara 1 SPS is depicted in Figure C.1 in Appendix C.

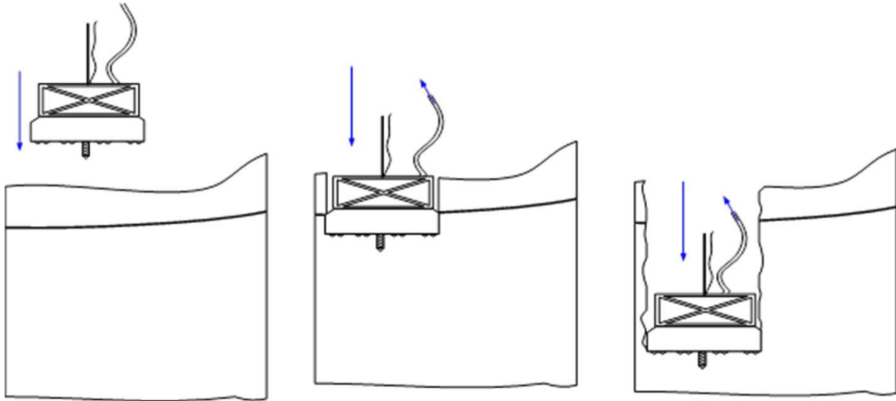


Figure 2.1: Illustration of vertical trench cutting method [7, p. 11].

2.2.2 BAUER and Technip Vertical Miner

An alternative to the Nautilus Minerals SPS is to use a vertical trench cutter system, similar to those used in onshore and shallow water mining applications. Since 2009, the french oil service company Technip¹ has led an R&D project on subsea mining, along with IFREMER (French Research Institute for Exploitation of the Sea) and ERAMET (a French mining and metallurgical group) [7]. Technip is also the main contractor of the Nautilus Minerals RALS. Technip Engineering has studied several mining methods, and concludes that a solution with a vertical continuous excavator seems highly promising. Reference [8] presents the results of a collaboration between Technip, BAUER Maschinen and the University of Delft. The paper presents a preliminary design of a vertical cutting tool able to work under hyperbaric conditions. An illustration of vertical trench cutting is shown in Figure 2.1. BAUER Maschinen has relevant experience as the company has provided vertical trench cutters for onshore applications since the 1980s [9]. Bauer has also delivered offshore cutters for diamond sampling off the coast of Namibia [7].

The vertical cutter system presented in [8] is depicted in Figure C.2 in Appendix C. Unlike the Nautilus Minerals SPS, uses this system a vertical mining approach based on onshore trenching technology. The vertical cutter is made up of a heavy steel frame fitted with two cutter drums. The two cutter drums rotate in opposite directions and are equipped with cutter teeth. The cut material is conveyed towards the opening of a suction box placed in the steel frame of the trench cutter. A sketch of the trench cutter is shown in Figure 2.2.

¹In 2017 FMC Technologies and Technip merged to TechnipFMC (<http://www.technipfmc.com/en/who-we-are>)

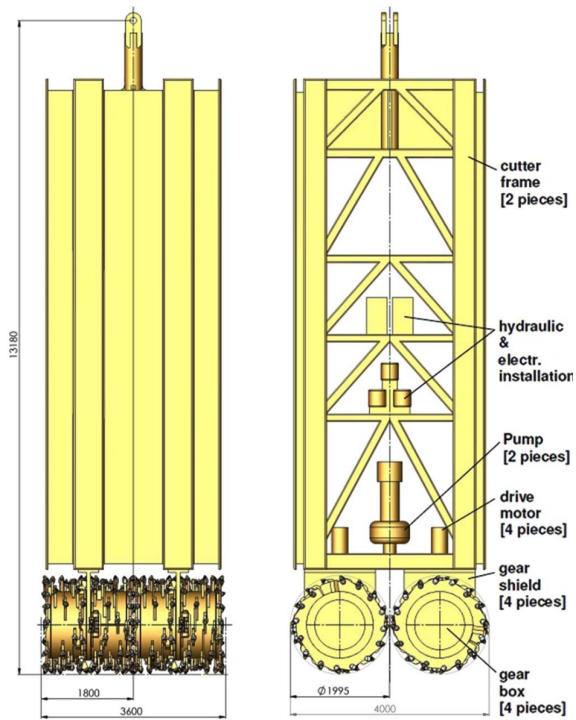


Figure 2.2: Sketch of the vertical cutter developed by BAUER and Technip for DSM applications. All measurements are in mm [8, Fig. 10].

2.3 Deep Sea Mining System Components

The different components of the presented SS, UTS and TS are described in this section. A summary of the different components' installed power is given in Table 2.2.

2.3.1 Seabed System

The SS is designed to cut, process, collect and transfer ore at the ocean floor. This requires the subsea mining tools to be equipped with an electrical machine capable of delivering several hundreds of kW to the cutter head of the machine. In addition to this, the mining tool will need a pump system which provides suction, i.e. a system capable of collecting and lifting the subsea slurry, in order to collect and transfer the ore to the UTS. In order to provide suction a centrifugal pump is required [2].

2.3.1.1 Nautilus Minerals Solwara 1 SS

The SPTs of the Solwara 1 project are all build with a mining tool, a centrifugal pump and track drive systems. The system is designed for an operational depth of 2,500 m. There are three different SPTs: an Auxiliary Cutter (AUX), a Bulk Cutter (BC) and a Collection Machine (CM). The AUX is designed to prepare the mining site for the BC, which mines the prepared area. Both tools are equipped with pumps in order to remove the cut material [10]. The two tools can pump the cut material away from the mining site, or to a stockpiling hood where the CM collects the ore and pumps it to the UTS. Reference [1] presents an estimation of the share of the installed capacity each part of the different SPTs have. The estimations of the different components share of the installed power are based on [11] and [12], the patents of the AUX and the BC respectively. Reference [11] states: "*The umbilical cable provides electrical power to drive the motors and pumps required to drive the main components of the AUX, such as track drive motors, hydraulic system drive motor(s), dredge system pump drive motor(s) and the cutter drive system*". Reference [12] states: "*The machine (...) delivers about 900 kW to the rock face (...)*" which indicates that the drum cutter of the BC requires at least 900 kW of the total installed capacity of 2.5 MW. Likewise for the AC, the patent ([11]) states: "*The rock cutter head is of about 600 kW power (...)*" which corresponds to 30 % of the AC total installed capacity of 2 MW [1, p. 32]. A similar, but slightly alternated, estimation is presented in Table 2.1.

The installed power of the SPTs pumps are based on information from [2] and [13], and is calculated to be in the range of 750-900 kW in order to be able to maintain the required flow rate of approximately 818 m³/h. See Appendix B. The CM mining tool installed power is assumed to be 20 % as the track drive systems and auxiliary systems, such as various control systems and boom hydraulics, are assumed to be the same percentage (30 %) for all SPTs as this is related to their size and weight.

	AUX	BC	CM
Part of SPT	Share of installed capacity		
Mining tool	30 %	40 %	20 %
Pump drive	40 %	30 %	50 %
Track drive and auxiliary systems	30 %	30 %	30 %
Installed power	2.0 MW	2.5 MW	1.8 MW
Weight	240 t	280 t	180 t

Table 2.1: Estimated share of total installed power for the Solwara 1 SPT components.

2.3.1.2 Vertical Miner SS

The vertical miner system, developed by BAUER and Technip, is designed for a production rate of approximately 130 t/h, which is roughly half of the Solwara 1 estimated production rate [2, 8]. In order to obtain this production rate the installed power for the cutter system is calculated to be 480 kW. The weight of the double trench cutter is estimated between 140 and 155 tons.

Compared to the Solwara 1 subsea components, the vertical cutter is approximately 50 % of the AUX and BC installed power of the mining tool and total weight. This implies that by operating two vertical trench cutters the same production rate as the Solwara 1 system is obtained. Reference [8] does not present any power consumption estimates for a pump system on the vertical trench cutter, but it states: ” ...*(the cuttings) are conveyed toward the openings of the suction box, from where they are pumped by a centrifugal pump through the slurry pipe incorporated in the cutter’s frame, via the mast head into the slurry conveying system ...*”, which indicates that the cutter frame is equipped with a centrifugal pump system in order to transport the ore-slurry to an UTS.

2.3.2 Underwater Transportation System

The UTS can, as mentioned, be driven by one or several pumps, located either topside, subsea or in intervals along the UTS riser pipe. Reference [13] investigates three different solutions for the vertical slurry transfer of the Nautilus Minerals Solwara 1 system. These solutions are presented below.

2.3.2.1 Centrifugal Pump System

The first method proposed is using centrifugal pumps in series along the riser transfer pipe. For an operational depth of 2,500 m the total pressure required to lift the 12 % ore-slurry can be as high as 90 bars. As the pressure head of a centrifugal pump is limited to about 12 bars the riser system would require eight pumps in series. There are several issues regarding such a high number of pumps. For instance, in order to assure redundancy for the riser system, by-pass valves would be needed for all pumps in case of the failure of one pump. As the centrifugal pumps would be exposed to a complicated three phase flow the volumetric concentration of ore

would be reduced, and the total efficiency of the system would decrease (compared to the PDP described in Chapter 2.3.2.3).

2.3.2.2 Air Lift System

Another solution is to use an air/gas lift system, which pumps compressed air or gas into the base of the riser pipe. As the compressed air/gas is injected into the riser, the gas will expand. This induces a lifting force in the slurry due to a reduction in the relative density of the fluid [2, 13]. An airlift system has advantages such as a low number of subsea components, which improves reliability and reduces maintenance. It is also a simple system, but due to the working principles of the system the flow rate would be too low and require large riser joints. In addition the equipment required to generate the volumes of gas to lift the slurry would require scarce vessel space, and the high power requirement would lower the efficiency of the entire UTS [13, 14].

2.3.2.3 Positive Displacement Pump

The third option for slurry transportation presented in [13] is to use a modified positive displacement pump, originally designed for dual gradient drilling applications. This is the solution selected for the Solwara 1 SPS and the positive displacement pump is called a SSLP, as mentioned in Chapter 2.2.1. The following description of the SSLP is an edited excerpt from [1].

The SSLP is designed with respect to several operational conditions, such as ambient pressure environment, ability to process a fluid with fluctuating concentration of solids, non-uniform flow conditions and varying viscosity and density of slurry [13]. All these factors affect the ability of the SSLP to maintain a required flow rate in order to successfully transport the ore to the PSV. The SSLP design is based on a Dual Gradient Drilling mudlift pump. Reference [13] states: "*In drilling for oil and gas, viscous fluid, or drilling mud, is used as a lubricant, coolant, and most importantly as a transport media to carry the cuttings created during the drilling process from the wellbore to a surface drilling vessel*". The circulation of the drilling mud has several similarities to the transport of the slurry in DSM, although parameters such as specific gravity and flow regime are very different between the two. In Dual Gradient Drilling a positive displacement pump is used to circulate the drilling mud. This pump is driven by pressurized seawater, pumped from the topside installation. The positive displacement pump consists of several chambers which are operated in order to maintain a continuous flow and avoid pulsations in the riser. Each chamber is equipped with a set of mud valves, controlled by subsea HPUs, in order to control the flow of slurry. The operation of a positive displacement pump is described in [13].

For DSM application, [13] concludes that a total of six 1,600 hp triplex pumps are sufficient to drive the SSLP and a total of ten chambers

will give required slurry flow rate through the SSLP. Reference [15] recommends a total of eight triplex pumps, six in constant operation and two spare, in order to power the SSLP. The overall power requirement for the SSLP will, according to [15], be less than 6.0 MW for operation at 2,500 m and less than 4.0 MW for operation at 1,700 m [1, Chap. 3.2.1].

2.3.3 Topside System

The only known concept of a DSM TS is the Nautilus Minerals PSV. The following description of a TS is therefore based on the description of the Nautilus Minerals PSV presented in [1]. The TS of a DSM system is the main component of the system, and the operational base for the mining operations. The TS is located on a surface vessel which can be defined as a combination of a bulk carrier and a support vessel. The components of the SS are stored and operated from the TS and deployed and retrieved from the TS using the SPT own LARS. Each LARS is driven by a HPU with a total installed power of approximately 2.2-2.4 MW. The UTS riser pipes are stored on board the vessel, and they are assembled and disassembled using a conventional derrick, similar to the ones used in O&G industry.

In addition to the SS and UTS handling systems the TS contains an ore dewatering plant and ore storage- and handling systems. This enables the TS to store up to 45,000 t of ore in the hull of the ship. The handling system allows the TS to offload ore to a bulk carrier without leaving the mining site. According to [10] these systems have a total installed power of 1.5 MW.

The total installed power of the PSV propulsion system is 20 MW. This makes the electric propulsion system the largest consumer of electric power. The installed power is divided by three azimuth thrusters located in the aft of the ship (each with an installed power of 3,000 kW), two azimuth thrusters located in the fore of the ship (each with an installed power of 3,500 kW) and two bow thrusters (each with an installed power of 2,000 kW).

The power generation of the DSM system is located topside on the PSV. For the Nautilus Minerals SPS the total power generation of 31 MW is provided by six diesel-generator sets of equal power, which are located in three groups of two in order to fulfill requirements of redundancy.

	Component	No of units	Installed Power (per unit)
TS	Diesel-Generator set	6	$\simeq 5.2$ MW
	Azimuth Thruster (Fore)	2	3.5 MW
	Azimuth Thruster (Aft)	3	3.0 MW
	Bow Thruster	2	2.0 MW
	LARS	3	2.2 - 2.4 MW
	Ore dewatering/handling	1	1.5 MW
UTS	Triplex pump	6	1,200 kW ($\simeq 1,600$ hp)
SS	AUX Centrifugal Pump	1	800 kW
	AUX Mining Tool	1	600 kW
	AUX Track Drive ++	1	600 kW
	BC Centrifugal Pump	1	750 kW
	BC Mining Tool	1	1,000 kW
	BC Track Drive ++	1	750 kW
	CM Centrifugal Pump	1	900 kW
	CM Mining Tool	1	360 kW
	CM Track Drive ++	1	540 kW
	Vertical Cutter Head	2	480 kW

Table 2.2: Installed power of the DSM system components designed for operation at 2,500 m depth.

Chapter 3

Theory

3.1 Power Quality in Offshore Grids

Electrical power systems for DSM application will be isolated power systems, as the distance from land excludes the possibility of grid connection to shore. This makes the electrical power system more fragile to disturbances from the installed elements (such as harmonic content and voltage-, frequency- and load variations) since the power system can not be interconnected with other power systems [1]. Therefore a high power quality is essential in order to assure security of electricity supply. The following is an excerpt from [1], describing power system reliability and quality:

Electrical power systems, both traditional and offshore, are required to guarantee a reliability of supply of high quality power. According to [16], electrical power of good quality is provided by:

- regulated and defined voltage levels with low fluctuations;
- a regulated and defined value of frequency with low fluctuations;
- low harmonic content.

Reference [16] suggest two basic methods of providing this quality: *”proper use of automatic voltage and frequency control methods”* and secondly; *”employing large, interconnected, power systems which, by their very nature, are less susceptible to load variations and other disturbances”*. When designing an isolated offshore power systems the latter method is impossible, making the first method for improved power quality an essential design criteria for offshore power systems. In addition to the quality of the delivered power, a high reliability of supply can (according to [16]) be ensured by:

- high quality of the installed elements;
- the provision of reserve energy;
- employing large interconnected power systems capable of supplying each consumer via alternative routes
- a high level of system security.

For offshore power systems, defined voltage levels and frequency values are easy to implement as the different parts of the power systems usually have explicit tasks, e.g. to supply industry- or hotel loads or provide a specific sending voltage to a

transmission cable. The harmonic content is however more complicated to limit as increased implementation of power electronic converters produces disturbances by distorting the power system waveforms, producing electromagnetic interference (EMI) [17]. This is further discussed below, in Chapter 3.1.1.

In addition to this, system security is important to ensure a high reliability of supply [16]. Reference [18] defines security of electricity supply as: " ... *the ability of the electrical power system to provide electricity to end-users with a specified level of continuity and quality in a sustainable manner, relating to the existing standards and contractual agreements at the points of delivery.*". As [19] emphasizes; this definition, and many others, is generally developed and optimized for traditional interconnected AC power systems. However, there are several indices for traditional on-shore AC grids that are applicable for offshore power systems. The reliability of a power system can be defined as the level of probability the power system has of fulfilling the power supply task adequately. This level of probability can be defined by indices such as the systems average failure rate and average outage duration [19]. By studying this indices one can evaluate the *quality of the installed elements, provision of reserve energy and level of system security*, as defined by [16], in order to ensure a high reliability of supply for the offshore power system.

Acceptable electric power quality is essential to be able to operate any offshore power system in a safe matter. As [20] states:

The quality of electric power (i.e. voltage supplies) is absolutely crucial to the operational integrity and safety of any land-rig, offshore drilling rig/ship or offshore installation, irrespective of type or class. Any failure or malfunction of equipment due to poor power quality can result in expensive downtime or, in a worst case scenario, severe or disastrous consequences.

Poor power quality may affect the installed equipment in such a way that it appears as a menace to the operation of the installation the electric power system is powering. Reference [20] exemplifies explosion-proof motors as such hazard. For such motors extensive exposure to current harmonics may affect thermal properties of the insulation material as the rotor (and other parts) are heated due to higher currents. This may further lead to excessive wear on mechanical parts, e.g. motor bearings, as a result of degraded lubrication. According to [20] a combination of excessive harmonic voltage distortion, non-sparking compressor motors with double cage rotors (i.e. which can attain high temperatures in the presence of harmonics) and the escape of condensate may have been the reason of the fatal Piper Alpha accident in 1988 in Scotland.

However, as the implementation of harmonic-generating equipment has increased over the last years, international standards regarding harmonics have increased accordingly. This is further discussed in Chapter 3.1.1.

3.1.1 Harmonic Content

Reference [21] defines harmonics as: " ... AC voltages or currents whose frequency is an integer of the fundamental grid frequency. Harmonic distortion refers to the effect of the fundamental waveform of non-sinusoidal or higher frequency voltage or current waveforms resulting from the operation of electrical equipment using solid state switches".

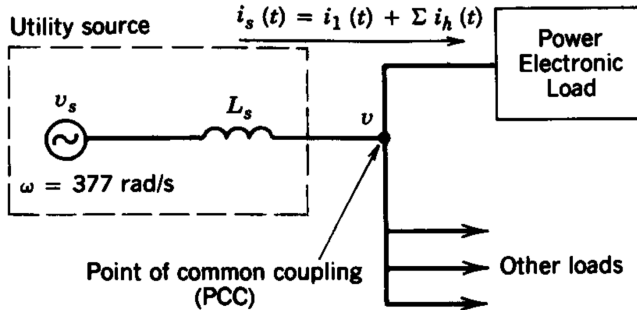


Figure 3.1: Utility source, power electronic load and other loads connected to a PCC [17, Fig 18-1].

In order to understand current harmonics Figure 3.1, Figure 3.2 and equations from [17] is presented. Figure 3.1 shows a utility source, a power electronic load and other loads connected to a point of common coupling (PCC). The voltage source v_s is represented with a finite (nonzero) internal impedance L_s connected to the PCC, thus the voltage at the PCC will be distorted. As a power electronic load is also connected to the PCC the current from the utility source i_s will not only contain the pure (fundamental) sinusoidal i_1 but also a sum of its harmonic (Fourier) current components $\sum_{h \neq 1} i_h$. The source current is given as

$$i_s(t) = i_1(t) + \sum_{h \neq 1} i_h(t) \quad (3.1)$$

were i_h is the harmonic current component at the h harmonic frequency $f_h (= hf_1)$. Figure 3.2 shows a distorted line current i_s (whole line) made up of the pure sinusoidal fundamental component i_{s1} at the line-frequency f_1 ($h = 1$) (dotted line) and the sum of all harmonic current components $i_{dis} (= \sum_{h \neq 1} i_h)$ at harmonic frequencies above the fundamental. In Figure 3.2 the voltage v_s is assumed to be pure sinusoidal, i.e. there are no voltage harmonics above the fundamental frequency.

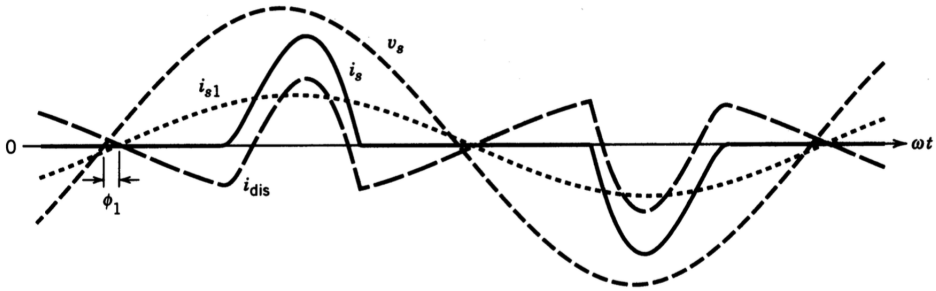


Figure 3.2: Distorted line current made up of fundamental current and distorted harmonic pollution [17, Fig. 3-5].

The distortion of the voltage v at the PCC depends on the internal impedance of the source and the magnitudes of the current harmonics injected into the source. As the internal impedance is (in principal) highly inductive it is represented by L_s . The RMS harmonic voltage at the PCC at a harmonic h of the line frequency ω is

$$V_h = (h\omega L_s)I_h \quad (3.2)$$

where I_h is the h harmonic current injected to the AC utility source. L_s can be defined by the short-circuit (per phase) fault current I_{sc} at the PCC. This current is the per-phase RMS current supplied by the utility source to a three-phase to ground fault at the PCC.

$$I_{sc} = \frac{V_s}{\omega L_s} \quad (3.3)$$

where V_s is the RMS value of the per-phase internal (assumed sinusoidal) voltage of the AC source. A larger value of I_{sc} will indicate a larger capacity of the total AC system at the PCC.

In order to quantify the amount of harmonic pollution in a current waveform an index called the total harmonic distortion (THD) is used. The THD is defined as the ratio between the sum of all harmonic current RMS values and RMS value of the fundamental current component.

$$THD = \frac{\sqrt{\sum_{h=2}^{\infty} I_h^2}}{I_1} \quad (3.4)$$

A similar index can be made for the voltage distortion by substituting the components in Equation 3.4 with the corresponding voltage components.

$$THD_v = \frac{\sqrt{\sum_{h=2}^{\infty} V_h^2}}{V_1} \quad (3.5)$$

For offshore power systems the harmonic content should be limited to certain values for different voltage levels according to international standards and marine classification societies, such as [22] and [23]. Reference [22] defines the voltage distortion limit for bus voltages in the range of 1-69 kV to 3.0% for individual harmonics and 5.0% for the THD_v. For offshore application the acceptable limits are somewhat higher. Reference [23] states:

In distribution systems the acceptance limits for voltage harmonic distortion shall correspond to IEC 61000-2-4 Class 2. (IEC 61000-2-4 Class 2 implies that the total voltage harmonic distortion shall not exceed 8%.) In addition no single order harmonic shall exceed 5%.

IEC 61000-2-4 is the standard for industrial and non-public power distribution systems at nominal voltages up to 35 kV and a nominal frequency of 50 Hz or 60 Hz. These values may be exceeded under the condition that the components exposed to the increased THD_v are designed to withstand the actual level of exposure.

The harmonic voltage can also be expressed (in percentage) as a ratio of the nominal system voltage V_s . Combining Equation 3.2 and Equation 3.3 gives:

$$\%V_h = \frac{V_h}{V_s} \times 100 = h \frac{I_h}{I_{sc}} \times 100 \quad (3.6)$$

By dividing both currents in Equation 3.6 with the fundamental current component I_1 of the source current the equation shows that for an increased ratio I_{sc}/I_1 a higher value of harmonic current I_h (in ratio to I_1) is acceptable without increasing the voltage distortion.

$$\%V_h = h \frac{I_h/I_1}{I_{sc}/I_1} \times 100 \quad (3.7)$$

This confirms that a larger value of I_{sc} gives a larger capacity of the total AC system at the PCC. Reference [22] defines limits on the harmonic currents power electronic equipment and other nonlinear loads are allowed to inject into utility systems. The ratio I_{sc}/I_1 is used to define the different limits for each odd harmonic order h . The limits defined in [22] are cited in [17]. These limits are presented in Table 3.1.

I_{sc}/I_1	Odd Harmonic Order h (%)					THD (%)
	$h < 11$	$11 \leq h \leq 17$	$17 \leq h \leq 23$	$23 \leq h \leq 35$	$35 \leq h$	
<20	4.0	2.0	1.5	0.6	0.3	5.0
20 - 50	7.0	3.5	2.5	1.0	0.5	8.0
50 - 100	10.0	4.5	4.0	1.5	0.7	12.0
100-1000	12.0	5.5	5.0	2.0	1.0	15.0
>1000	15.0	7.0	6.0	2.5	1.4	20.0

Table 3.1: Allowed harmonic current distortion for equipment [22, Table 2].

Notes (cited from [17, Table 18-2]):

Harmonic current limits for nonlinear load connected to a public utility at the PCC with other loads at voltages of 2.4 - 69 kV.

I_{sc} is the maximum short-circuit current at PCC.

I_1 is the maximum fundamental frequency load current at PCC.

Even harmonics are limited to 15% of the odd harmonic limits above.

3.1.2 Power Factor

When transferring active power from an AC source to a load the current components at harmonic frequencies do not contribute to the active power transfer. The active power P transferred, e.g. from the utility source to the loads in Figure 3.1, is given by

$$P = V_s I_1 \cos \phi_1 \quad (3.8)$$

where ϕ_1 is the phase angle between the (assumed sinusoidal) voltage v_s and the fundamental component i_1 (shown in Figure 3.2) and V_s and I_1 are the RMS values of v_s and the fundamental component i_1 , respectively. The apparent power S from the source is given by the product of the RMS voltage V_s and the RMS current I_s

$$S = V_s I_s \quad (3.9)$$

where the RMS-value of the source current is given by

$$I_s = \sqrt{I_1^2 + \sum_{h \neq 1} I_h^2} \quad (3.10)$$

The displacement power factor (DPF) is defined as the cosine of the angle ϕ_1

$$DPF = \cos \phi_1 \quad (3.11)$$

which is the same as the power factor (PF, given as P divided by S) in linear circuits with sinusoidal voltages and currents, i.e. the source current $i_s(t)$ contains no harmonics. For non-linear circuits the PF is also given as P divided by S:

$$PF = \frac{P}{S} = \frac{V_s I_1 \cos \phi_1}{V_s I_s} = \frac{I_1}{I_s} \cos \phi_1 = \frac{I_1}{I_s} DPF \quad (3.12)$$

By studying the equation it is clear that a large distortion of the current will result in a low PF. Hence, in an AC power system with a low PF the current will have a lower capability of transferring active power as the harmonic components will 'occupy' the capability of the installed equipment, e.g. current rating of transformers and thermal limits of cables. By substituting Equation 3.4 into Equation 3.12 the PF can be expressed as

$$PF = \frac{1}{\sqrt{1 + THD^2}} DPF \quad (3.13)$$

which shows that as the THD increases the PF decreases, accordingly any power system should minimize the THD in order to improve the operating PF.

3.2 Reactive Power Compensation and Harmonic Content Reduction

There are different ways of reducing the harmonic content in power systems. In order to reduce the influence of harmonic content one may implement a shunt active power filter (APF) as described in [24]. Different power filters can be used to filter harmonic currents and improve the PF of an AC system. Two types of active shunt compensation devices are described below.

3.2.1 SVC and STATCOM

This Chapter (3.2.1) is an edited excerpt from [25].

There are, according to [17], three types of static var controllers: thyristor-controlled inductors (TCIs), thyristor-switched capacitors (TSCs) and switching converters with minimum energy storage elements. TCIs are more commonly called Thyristor-controlled reactors (TCRs). TSCs and TCRs in a hybrid configuration is referred to as SVC (Static VAR Compensator), and switching converters as STATCOMs [26]. TSCs and TCRs are made up of, respectively, capacitors and inductors connected to the source through two back-to-back connected thyristors. See Figure 3.3. It is possible to connect both the SVC and the STATCOM in series or shunt to the system. This section will only consider shunt connected SVC and STATCOM as its application will be for isolated offshore power systems.

3.2.1.1 Thyristor controlled reactors (TCRs)

The TCRs are controlled by varying the thyristors firing angle α . By analyzing Figure 3.3a, the following equation can be developed for the RMS-value of the fundamental current I_{L1} [17, p. 473]:

$$I_L = I_{L1} = \frac{V_s}{\omega L} \quad (3.14)$$

where $\omega = 2\pi f$. Since the current is sinusoidal and inductive it lags the voltage by 90° . Thus, controlling the firing angle α in the range $0-90^\circ$ gives no control over i_L , but by increasing α beyond 90° reduces i_L due to the delayed commutation. This gives an effective control over the inductance which gives

$$L_{eff} = \frac{V_s}{\omega I_{L1}} \quad (3.15)$$

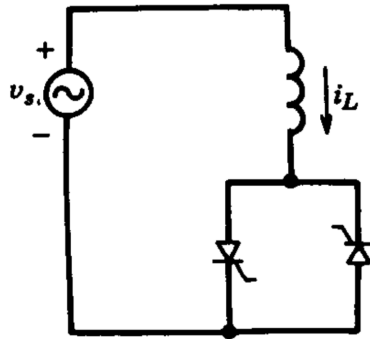
where I_{L1} is given (by Fourier analysis) as

$$I_{L1} = \frac{V_s}{\pi\omega L} (2\pi - 2\alpha + \sin 2\alpha) \quad \left(\frac{1}{2}\pi \leq \alpha \leq \pi\right) \quad (3.16)$$

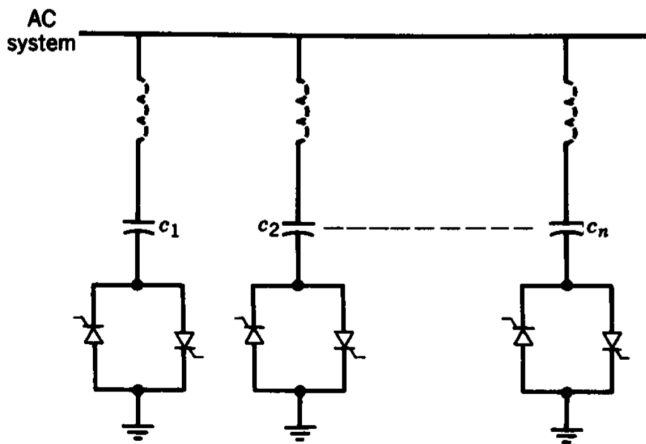
The total reactive power drawn by the per phase TCR is (at the fundamental frequency)

$$Q = V_s I_{L1} = \frac{V_s^2}{\omega L_{eff}} \quad (3.17)$$

This analysis is only valid for the fundamental current i_{L1} . Since the inductor current also consists of odd harmonics h of order 3, 5, 7, . . . it is common to Δ -connect three-phase TCRs so that these harmonics do not enter the ac system. It is also common to connect a capacitor in parallel to filter out high frequency harmonics. This is the simplest structure of a var compensator capable of providing both inductive and reactive power [27].



(a)



(b)

Figure 3.3: Circuit equivalent of TCR (a) and TSCs (b), both shunt connected [17].

3.2.1.2 Thyristor switched capacitors (TSCs)

One TSC will only give two operating points for different voltages, depending on whether it is on or off. One can obtain more operating points by splitting the same capacitance among more parallel connected TSCs, as shown in figure 3.3b. By

giving the capacitors a binary configuration

$$c_1 = C, c_2 = 2C, c_3 = 4C, \dots, c_n = 2^{(n-1)}C \quad (3.18)$$

it is possible to vary the reactive power Q_c in discrete steps [27, 17]. The inductors connected to the TSCs in figure 3.3b make sure the thyristors start conducting at the currents zero-crossing if the turn on occurs at the grid maximum voltage. This is to protect the thyristors from destructive effects.

3.2.1.3 STATCOMs

A STATCOM is a converter-based VAR generator, consisting of a DC voltage source and a voltage source inverter, that instantaneously generates reactive currents. A controller measures the AC system and controls the switching of the IGBTs in the voltage source inverter [17]. A STATCOM can also have the ability to exchange both real and reactive power if it is equipped with an energy storage device at the DC-terminals [28].

Compared to SVC the STATCOM is smaller in size, faster and it performs better at lower voltages [27]. Although STATCOMs have better performance, SVCs are often used due to lower investment and operational costs [29]. A comparison of the V-Q characteristics of the SVC and the STATCOM is given in figure 3.4.

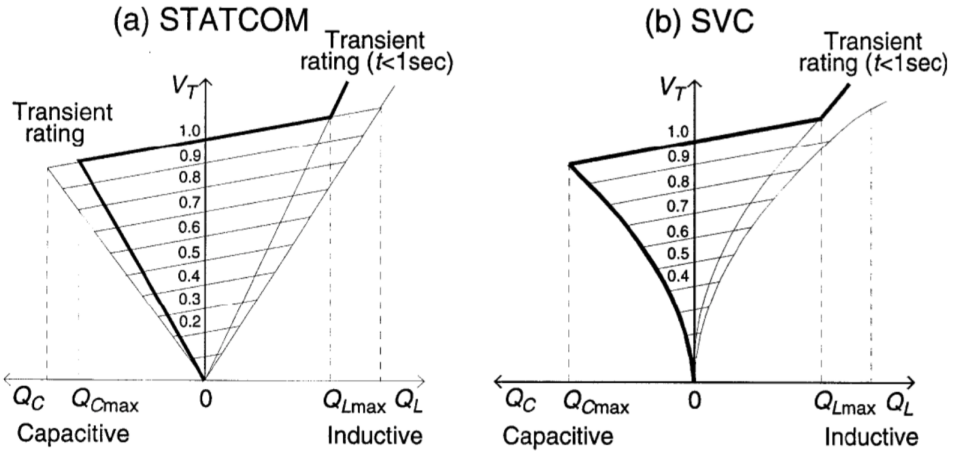


Figure 3.4: V-Q characteristics of the SVC and the STATCOM [27].

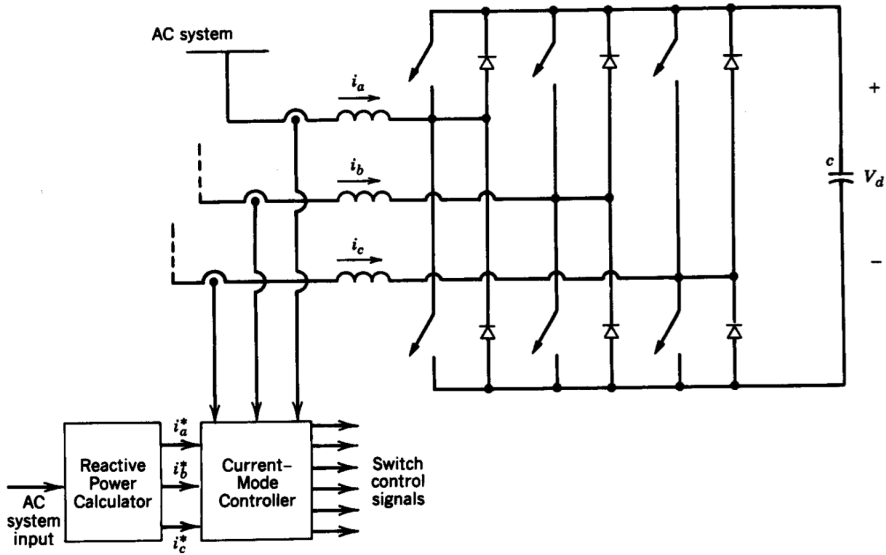


Figure 3.5: STATCOM with a Current-Mode Controller [17].

3.2.2 Control of APF

In order to control the switching of the compensation device different control techniques are applicable. In Figure 3.5 a current-mode controller is used to control the switching of the switches in the voltage source inverter. The controller receives reference signals from the reactive power controller and compares this to the actual waveforms of the AC system. Then the harmonics in the AC system are cancelled by the resulting reactive currents made by the voltage source inverter.

3.3 Cables

This Chapter (3.3) is cited from [1].

When modeling subsea cables the medium cable length model, often referred to as *the nominal π -equivalent circuit*, is used. Medium length cables are defined as lines between 80 and 250 km [16], but subsea cables should always be modelled with shunt capacitors due to the capacitance of the cable [30]. Compared to overhead lines the charging current of a cable is about 30 times larger [16]. The per-phase π -equivalent circuit is shown in Figure 3.6. In the model, half of the cable shunt capacitance is considered to be lumped at each end of the cable.

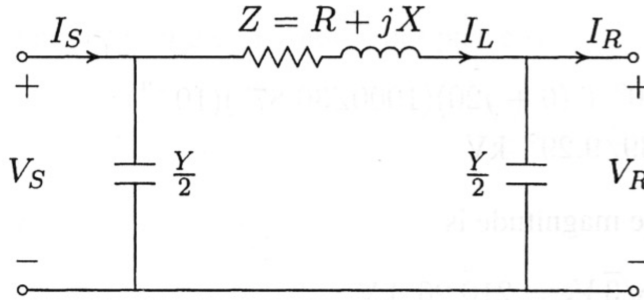


Figure 3.6: The nominal π -equivalent circuit of a medium length transmission line [31, p. 80].

The impedance Z is given by Equation 3.19 and the admittance Y by Equation 3.20. V_S , I_S , V_R and I_R are the sending and receiving end phase voltages and currents. I_L is the current through the series impedance.

$$\begin{aligned} Z &= (r + j\omega L)l \\ &= R + jX \end{aligned} \quad (3.19)$$

$$\begin{aligned} Y &= (g + j\omega C)l \\ &= G + jB \end{aligned} \quad (3.20)$$

The different cable parameters given in the equations are explained in the nomenclature and $\omega = 2\pi f$ where f is the frequency of the sending end voltage and current.

The loading of subsea cables is often compared to the cable's *surge impedance loading* (SIL). According to [16], SIL is defined as "the power delivered at rated voltage to a load impedance equal to the characteristic impedance of a transmission line" assuming a flat voltage profile, which yields $V_s = V_R$. For subsea cables the SIL corresponds the loading of the cable P_{SIL} at which natural reactive balance occurs. This means that the cable's produced reactive power Q_{prod} is equal to the cable's consumed reactive power Q_{cons} . When assuming a loss-less line, g and r are neglected giving $Y = B = \omega C \cdot l$ and $Z = X = \omega L \cdot l$. The produced reactive power

(due to cable capacitance) and consumed reactive power (due to cable inductance) can be calculated by Equation 3.21 and 3.22 respectively [32]:

$$Q_{prod} = V_n^2 \cdot Y \quad (3.21)$$

$$Q_{cons} = 3I_L^2 \cdot X \quad (3.22)$$

where V_n is the nominal (line-to-line) RMS voltage of the cable. By putting $Q_{prod} = Q_{cons}$ and solving the equation for I_L the current at SIL is found to be:

$$\begin{aligned} Q_{prod} &= Q_{cons} \\ V_n^2 \cdot Y &= 3I_L^2 \cdot X \\ I_L &= \sqrt{\frac{V_n^2 \cdot Y}{3 \cdot X}} \\ &= V_S \sqrt{\frac{Y}{X}} \\ &= V_S \sqrt{\frac{C}{L}} \end{aligned} \quad (3.23)$$

P_{SIL} can then be expressed as [30]:

$$\begin{aligned} P_{SIL} &= 3V_S I_L \\ &= 3V_S V_S \sqrt{\frac{C}{L}} \\ &= V_{LL}^2 \sqrt{\frac{C}{L}} \end{aligned} \quad (3.24)$$

where the characteristic impedance of the cable is given as:

$$Z_c = \sqrt{\frac{L}{C}} \quad (3.25)$$

If the active delivered power at the receiving P_R end is larger than P_{SIL} the cable will be a net consumer reactive power, and if P_R is smaller than P_{SIL} the cable will be a net source of reactive power. As Equation 3.24 shows; the SIL is independent of the cable length. However, the reactive power production increases with increased cable length. As cables usually have a very low characteristic impedance (compared to overhead lines) the thermal limit of the cable will limit the loading to values below P_{SIL} , resulting in subsea cables almost always being reactive power producers. If the reactive power production in the cable is too large this will limit the active power capability of the cable, as the transferred active power is depended of the cable active current capability and thermal limit. An illustration of the limitations in active current capability made by increasing the capacitive current is shown in Figure 3.7. The maximum current at the thermal limit, I_{TL} , is a natural limitation

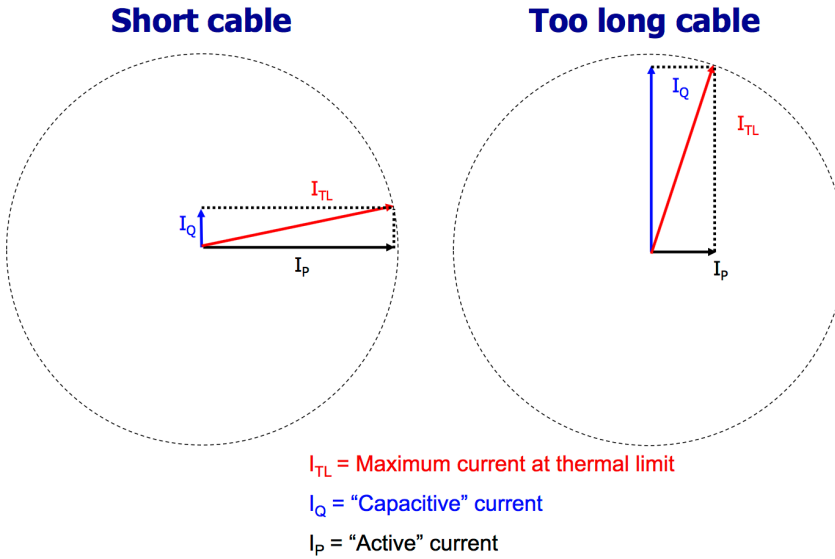


Figure 3.7: An illustration of the cable limitation in active power transfer due to reactive charging current [34].

of the cable as possible failure in the cable may occur due to insulation heating caused by dielectric losses [33]. The relation between the currents in Figure 3.7 is given in Equation 3.26.

$$I_{TL} = \sqrt{I_Q^2 + I_P^2} \quad (3.26)$$

where I_Q and I_P are the reactive (capacitive) and active part of the current. At a given length the reactive power produced reduces the cable's current carrying capability of transmitting active power to zero [32].

Chapter 4

Deep Sea Mining Power System Topologies and Modelling

This chapter will present a power estimation for all DSM system components in order to operate at a depth of 3,500 m depth. The different system topologies proposed in this thesis and their respective PowerFactory models are described and depicted in this chapter, along with the DSM system component representation in PowerFactory. Some reflections regarding the different designs and physical characteristics of the system components, costs and the different topologies utilization of available space, are presented in Chapter 6.2.

4.1 Power Estimation for DSM Operations in the Norwegian Sea

In order to simulate a DSM system for operations in the Norwegian Sea the power consumption of the different components must be estimated. As the Nautilus Minerals SPS is designed for an operational depth of 2,500 m, it is assumed that the values of installed power for the different components presented in Table 2.2 correspond to operation at this depth. For DSM operations in the Norwegian Sea the SMS deposit Loki's Castle, presented in Chapter 2.1.2, is the most promising location. This vent site is located at 2,400 m depth, but as SMS deposits are located at depths up to 3,700 m the presented system will be designed for an operational depth of 3,500 m. This implies that the umbilicals providing power to the SS will be 4 km long. It is reasonable to assume a higher power consumption for the TS due to harsh weather conditions in the Norwegian Sea as the significant wave height is approximately twice as high as in the Bismarck Sea [2]. The power estimation for operation at 3,500 m for the different components are presented in this chapter and summarized in Table 4.1.

4.1.1 SS

As the SPTs will operate at 3,500 m depth, an increase of 40 % compared to operations at 2,500 m, it is reasonable to assume a somewhat higher power demand. Reference [8] presents estimations for required cutting power for two mining sites at depths of 1,000 m and 2,000 m and compares it to atmospheric conditions (0 m). The results shows a linear trend between 0 - 1,000 m and a somewhat reduced increase in required cutting power between 1,000 - 2,000 m. Similar results are obtained by [35]. The installed power of the AUX, BC and CM cutter heads are therefore assumed to be approximately 30 % higher for operations at 3,500 m based on these references.

The centrifugal pumps of the SPTs will be assumed to have the same installed power as in the Nautilus Minerals SPS. This is because the distance from the seafloor to the SSLP will be unchanged with respect to operational depth, hence the power demand required for collecting and moving the cut material to the SSLP or the stockpiling hood is independent of the ambient pressure as it is the difference in height which decides the required power.

The track drive systems installed power is assumed to be about 50 % higher for operation at 3,500 m depth. This estimation is based on parameters such as drag in the increased ambient pressure and buoyancy and gravity forces due to higher weight of the SPTs. An increase in weight is to be expected as the SPTs will have an increased installed power of the mining tool and other construction parameters due to higher ambient pressure.

4.1.2 UTS

In order to adjust the UTS for operations at 3,500 m a linear dependency is assumed. As the 2,500 m system requires 6.0 MW the 3,500 m system is estimated to require 8.4 MW. According to [15] the *overall* power requirement of the 2,500 m system is 6.0 MW. Assuming that this power requirement of 6.0 MW includes losses, the 3,500 m system can be run by nine 1,600 hp triplex pumps operating at 80 % of installed capacity.

4.1.3 TS

The mining systems of the TS is assumed to have the same installed power as presented in Chapter 2.3.3. In addition, other ship loads such as ship hotel services and other auxiliary ship systems are estimated to require 1.0 MW. The LARS and the DP system are however assumed to require a larger installed effect as the SPTs are assumed to be heavier and the weather conditions in the Norwegian Sea rougher (compared to the Bismarck Sea where the Nautilus Minerals SPS will operate). In addition will other equipment, e.g. increased cable length, increase the total weight of the entire production system. The total installed thruster effect is therefore increased with 25 %. As the total installed power of the SPTs has increased with 25 % the same increase is assumed for the installed capacity of each diesel-generator set, which is increased to 8.5 MVA in order to handle the increased power demand

	Component	No of units	Installed Power (per unit)
TS	Diesel-Generator set	6	8.5 MVA
	DP	1	25 MW
	Ore dewatering/handling	1	1.5 MW
	Hotel loads and auxiliary systems	1	1.0 MW
UTS	Triplex pump	9	1,200 kW (\simeq 1,600 hp)
SS	AUX Centrifugal Pump	1	800 kW
	AUX Mining Tool	1	800 kW
	AUX Track Drive ++	1	900 kW
	BC Centrifugal Pump	1	800 kW
	BC Mining Tool	1	1,300 kW
	BC Track Drive ++	1	1100 kW
	CM Centrifugal Pump	1	900 kW
	CM Mining Tool	1	500 kW
	CM Track Drive ++	1	800 kW

Table 4.1: Installed power of the DSM system components designed for operation at 3,500 m depth.

of the power system. The LARS is not evaluated as it is omitted in the simulation models.

4.2 Different System Topology Configurations

In order to investigate the different possibilities of power distribution to seafloor mining equipment, several different simulation models have been made. When supplying the subsea machines with several megawatts of power the electric power system should be designed with respect to several issues. Minimizing voltage drop and distribution losses, robustness and redundancy of the system and reducing size, weight and cost of the equipment are often conflicting criteria, e.g. a reduction in weight and size often implies an increase in costs, or vice versa.

The Nautilus Minerals SPS is the only existing full-scale SPS for DSM and will be the basis for the DSM electrical power systems analyzed in this thesis. As the simulations will focus on the different system topologies the TS of the Nautilus Minerals SPS will be used for all simulations in all models. In addition, the UTS will be powered by topside pumps for all configurations. This decision is based on the information given in Chapter 2.3.2 and is further discussed in Chapter 6. The components of the SPTs will also be the same for all models.

Three simplified and four detailed models of possible DSM system topology configurations are presented below. There are two AC and two DC distribution models. A voltage level of 6.6 kV is chosen for the AC systems and ± 3.0 kV for the DC system. The AC voltage level is chosen based on information presented in [1]. The DC voltage level is selected to give a realistic comparison between AC and DC distribution. A fourth simplified model is also made in order to investigate the location of the motor converters. The simplified models are named 'Model A-D' and the detailed models 'Model 1-4'.

4.2.1 Simplified Models

To verify the chosen system topologies three simplified AC 60 Hz models are made. The first model simulates a production system where all SPT loads are powered individually by cables from the TS. This model is named 'Model A'. This allows for the motor frequency converters to be installed topside, in order to avoid expensive subsea installations. The second simplified model, named 'Model B', is similar to the Nautilus Minerals SPS. The third simple model (Model C) combines the power distribution by connecting all the subsea loads to one distribution station. A SLD of each model is presented in Figure D.1 in Appendix D.

The last simple model (Model D) compares the effects of having the frequency converter of a subsea motor topside on a vessel, versus in a subsea installation, i.e. either at the sending or receiving end of the cable. The simulation results of this model will be a supplement to the results of model A, B and C when designing the electric power system. A SLD of Model D is presented in Figure D.2 in Appendix D.

4.2.2 Model 1: Individual 60 Hz AC Distribution

The first simulation model is the Nautilus Minerals Solwara 1 system topology. This 'base-model' will be called Model 1 and the simulation results of the other models will be compared to the simulation results of Model 1. The system is an AC system with an electrical frequency of 60 Hz. Each SPT is supplied with power through its own umbilical so they can be operated independent of each other. This increases the total redundancy of the mining system as the production can continue if a fault or breakdown occurs in one of the SPT or its cable. The SPTs are modelled as a single AC subsea bus bar with all its components connected to it. Onboard the SPT the power is distributed to the different motors through designated converters located on the SPT. A SLD of the system topology is presented in Figure 4.1. Each cable providing power to the SPT buses are 4 km long 3-core copper cables.

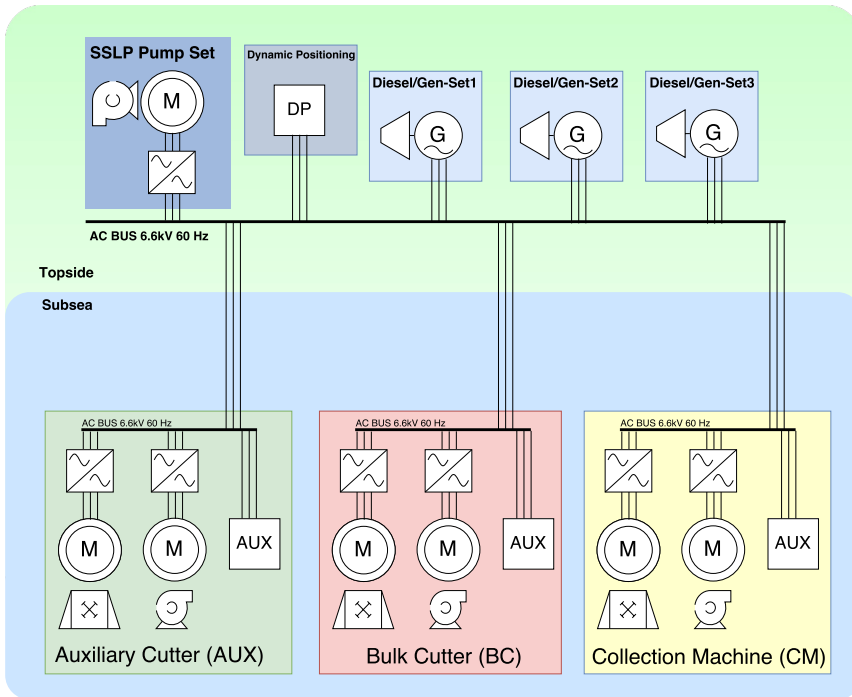


Figure 4.1: Model 1 SLD.

4.2.3 Model 2: Combined 60 Hz AC Distribution

The second model combines the power supply of the three SPTs. The power will be transferred to a common subsea installation, which distributes the power to the SPTs through designated cables. In this configuration the frequency converters of the motors can either be placed on board the SPT or in the subsea distribution station, the latter requiring a designated cable for each SPT component from the distribution station. In the simulation model the cable from the distribution station to the SPT is neglected in order to simplify the model. The power will be transferred through two 4 km long 3-core copper cables. The system topology is depicted in Figure 4.2.

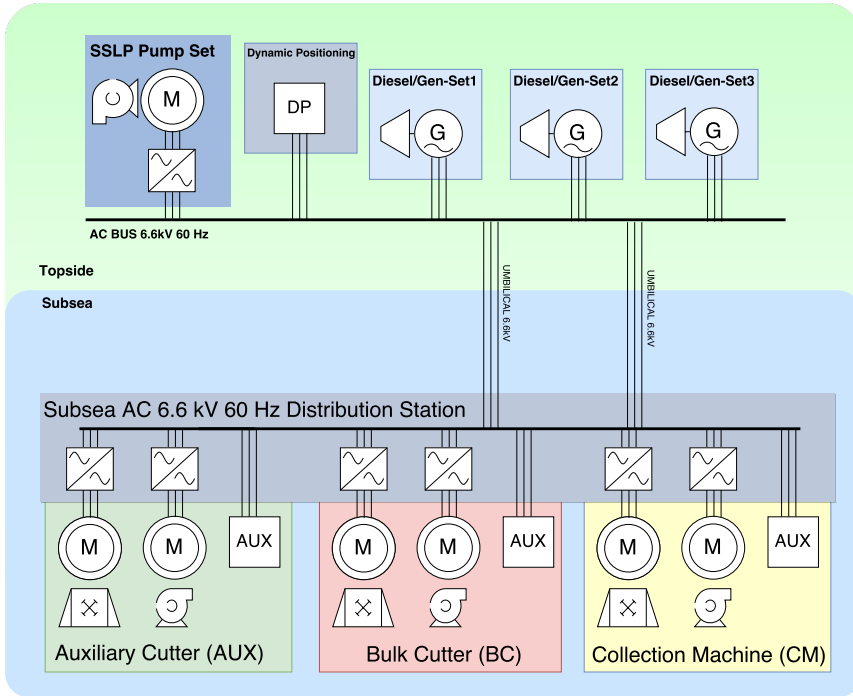


Figure 4.2: Model 2 SLD.

4.2.4 Model 3: Individual DC Distribution

Model 3 has the same design as Model 1, with individual power distribution to the SPTs, but with DC power distribution. DC distribution on ships is becoming a prominent alternative to the classical AC power systems [36, 37]. However, because of the maturity of AC technology, the TS is chosen to be AC. In this system a bipolar $\pm 3\text{kV}$ configuration is used as this is a recommended preferred rated voltage [38]. By utilizing a bipolar system the insulation of the cables can be designed for the peak voltage of 3kV as opposed to the AC system which has a peak (phase) voltage of 5.4kV . In order to obtain a DC voltage level of $\pm 3\text{kV}$ the AC voltage of 6.6kV is stepped down as the simulated rectifiers are passive rectifiers. Thus, the distribution voltage of Model 3 is comparable to that of Model 1.

Using DC distribution can be viewed upon as extending the DC-link of the frequency converters of the SPTs as the AC/DC conversion will be topside and the DC/AC conversion subsea. In the model each SPT will have a designated rectifier topside and two cables (one for each polarity) powering the SPT. It is assumed that the two cables can be bundled in the same umbilical. One-core copper cables are selected. The SPTs are modelled as two DC buses (one for each polarity) with each SPT motor connected to the buses through an inverter. A SLD of the system topology is depicted in Figure 4.3.

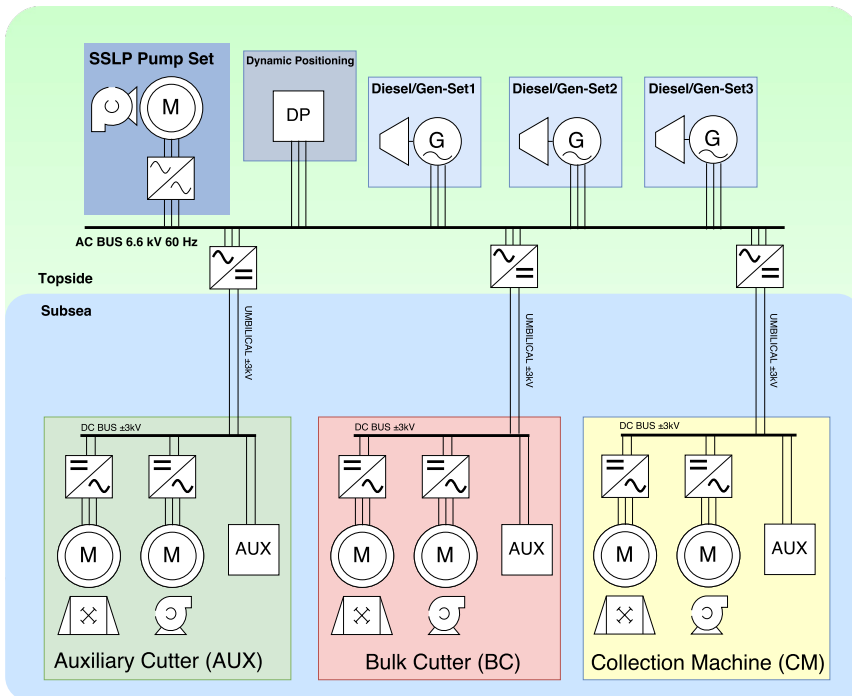


Figure 4.3: Model 3 SLD.

4.2.5 Model 4: Combined DC Distribution

The last model is similar to Model 2, but with DC distribution. As for Model 3; the TS is still AC and the topside rectifier is fed through a step-down transformer in order to simulate a DC system with a voltage level of $\pm 3\text{kV}$. The power is distributed to the DC subsea station through four cables (two for each polarity). The same type of cables as in Model 3 are used. A SLD is presented in Figure 4.4.

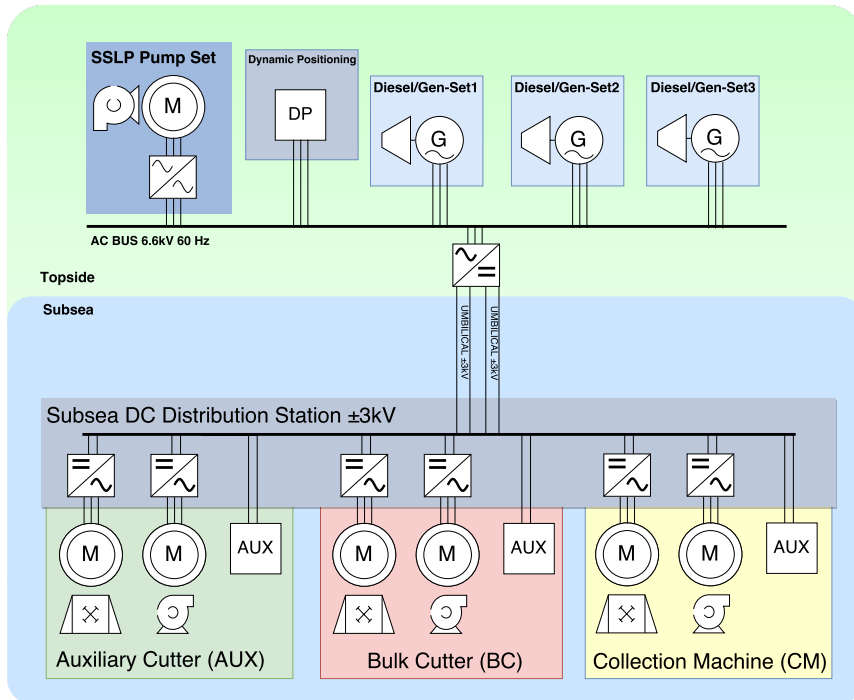


Figure 4.4: Model 4 SLD.

4.2.6 Modelling of SPT Components

In Model A, B and C each SPT is modelled by three simple passive loads rated with the installed power of the SPT component. All converters are omitted as the models are simplified in order to execute simple load flow analysis. In Model 1-4 the motors of the SPTs are modelled more accurately. The mining tool and the pump drive of the SPT are modelled as induction machines with a designated converter to each motor. The track drive system and auxiliary loads are modelled as an aggregated passive load similar to the ones in the simplified models. This is done in order to model the mining operation as accurate as possible, i.e. the SPTs are assumed to be at standstill during mining operations as the track drive system are modelled as passive loads. This is however not the case for the BC which will move during mining operations. Despite of this the BC track drive system is modelled as a passive load.

The machines used in the simulation software are single cage induction motors with a rated frequency of 50 Hz and rated voltage of 6 kV. The motor parameters are taken from [39], a catalogue of induction motors for use in hazardous locations in the chemical and O&G industry. Parameters of HV pressurized cast iron totally enclosed squirrel cage three phase motors are chosen in order to simulate the subsea motors of the SPT components. For the mining tools, 8-pole machines are chosen as the cutter heads of the mining tools require high torque at low speed. 2-pole machines are chosen for the motor for the centrifugal pumps. The motor specifications and type (from [39]) chosen for the different SPT components are presented in Table 4.2.

Component	Motor Type	Power kW	Speed r/min	Torque Nm	Inertia kgm²
AUX Centrifugal Pump Motor	HXR 500LH2	800	2987	2557	23.8
AUX Mining Tool	HXR 500LK8	800	745	10257	69.1
BC Centrifugal Pump	HXR 500LH2	800	2987	2557	23.8
BC Mining Tool	HXR 560LM8	1,250	746	16002	136.9
CM Centrifugal Pump	HXR 500LL2	900	2988	2877	27.0
CM Mining Tool	HXR 450LK8	500	744	6420	46.3
SSLP Pump Motor	HXR 560LM2	1,250	2986	3997	46.2

Table 4.2: The motor type (and specifications) chosen for the different SPT components and SSLP pump drive. Values are taken from [39].

4.2.7 Modelling of TS and UTS

In Model A - D the topside system is simulated as a 6.6 kV AC 60 Hz bus powered by an external grid. All TS components and the SSLP pump drive are omitted.

In Model 1 - 4 the TS is modelled as an AC bus with the components directly connected to it. In reality the TS electric power system would need different switchboards, circuit breakers, designated back-up generation and other essential electric infrastructure. However, as the purpose of the simulations is to study the DSM-aspect of the power system, simplifications are made. The generators are 6.6 kV salient pole synchronous generators. Each generator is rated at 8.5 MVA 0.85 PF. All three diesel-generator sets are equipped with AVR and turbine governors from the PowerFactory library.

As the focus of the simulations is with respect to the system topology of a DSM electric power system the TS is somewhat simplified. The LARS is neglected as it is not a consumer of power during the mining operations. Although the DP is the largest consumer of power in the production system the thrusters of the DP is simplified to one aggregated passive load as it will be similar for all the presented models. To be able to investigate the loading of the generators during mining operations a passive load representing the ore dewatering plant, UTS handling systems and other ship hotel and auxiliary loads are added to the TS.

The UTS is modelled as nine induction machines operating in parallel. These motors represent the previously discussed triplex pumps that drive the SSLP. Like the motors of the SPTs, the values for this machine are taken from [39] and presented in Table 4.2.

Chapter 5

Simulations and Results

5.1 Simple Models

The first simulations are done in order to verify the exclusion of each SPT component being supplied by its own umbilical as a possible system topology. Since the distance between the TS and SS is relatively short (compared to O&G step-out distances), it is possible to install the frequency converters of the motors on the TS installation, thus saving the cost of expensive subsea installations on the SPTs. This will also decrease operation and maintenance costs as the components will be easier to access. In order to have topside converters, each SPT component will need its own cable for power supply in order to control the motor.

5.1.1 Model A and B Load Flow Analysis

Since there is an economical incentive to have topside converters it is important to investigate the technical aspects of this configuration. A simple load flow analysis is therefore carried out on Model A and Model B. In order to differentiate the results the SPT components are loaded at 100 % of the installed capacity at 0.85 PF and the cables of the models are dimensioned to be loaded between 60-70 %. The resulting cable size, loading and voltage drop for the two models are presented in Table E.1 in Appendix E. The power infeed, power consumption and power losses are shown in Table 5.1 below.

		Model A	Model B
External Infeed	Active Power	8.55 MW	8.17 MW
	Reactive Power	4.91 MVar	5.11 MVar
	Apparent Power	9.86 MVA	9.64 MVA
Total Load	Active Power	7.90 MW	7.90 MW
	Reactive Power	4.90 MVar	4.90 MVar
	Apparent Power	9.30 MVA	9.30 MVA
Grid Losses	Active Power	0.65 MW	0.27 MW
	Reactive Power	0.01 MVar	0.21 MVar
Line Charging	Reactive Power	-0.11 MVar	-0.05 MVar

Table 5.1: Power loss in Model A and B.

The total active power loss in Model A is 650 kW, while in Model B it is 270 kW. This corresponds to 7.6 % and 3.3 % respectively. The active power loss of 7.6 % in Model A is very high and in addition to this, as presented in Table E.1, the voltage drop in the cables of Model A are between 6-7 % (except the CM Tool cable which, due to lack of smaller cables in the PowerFactory-library, is loaded at 37 %). Although the system design in Model A is simple and allows the converters to be installed topside, the large power loss and voltage drop makes the system less lucrative to operate, e.g. with respect to increased fuel consumption due to high active power losses.

5.1.2 Motor Start Up Analysis

In addition to the load flow analysis of Model A, B and C (a load flow analysis for Model C is presented in the next section) a motor start up simulation has been carried out for Model D. The simulated motor is somewhat similar to the SSLP pump drives in Model 1-4. The simulated machine is eight identical induction motors operated in parallel. The technical specifications of the motors are given in Table 5.2.

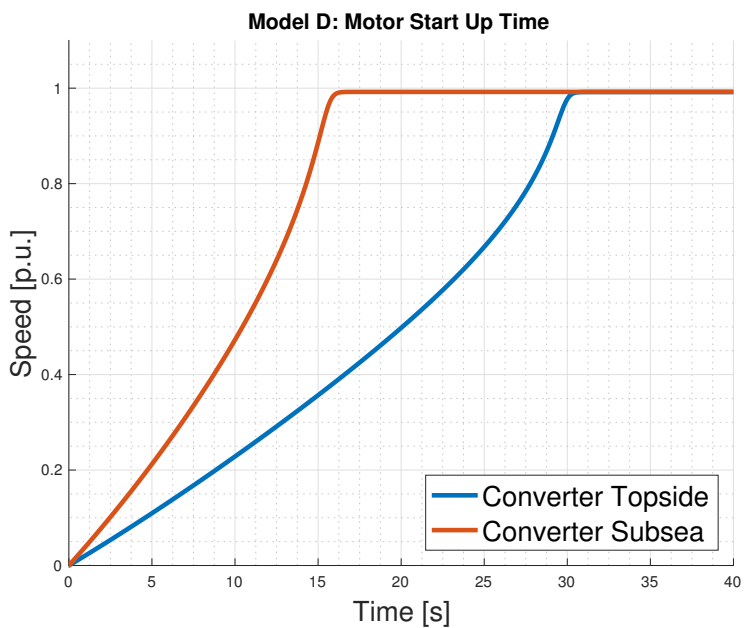
Rated Voltage:	6.6 kV
Rated Apparent Power:	1,304 kVA
Rated PF:	0.939
Nominal Frequency:	60 Hz
Moment of Inertia:	205 kgm ²
Number of Motors:	8

Table 5.2: Technical parameters of the motor in Model D.

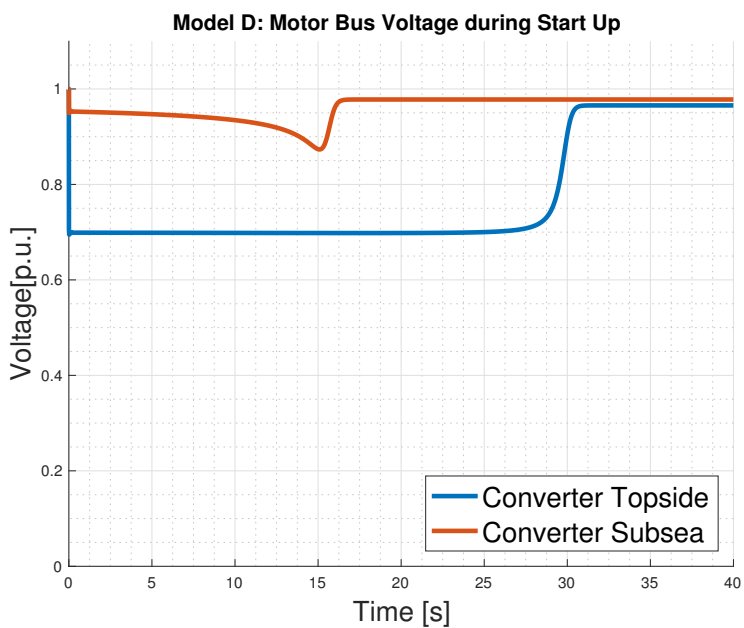
Two system configurations are simulated with a start up of the described machine. The power is supplied through two 3×300 mm XLPE-CU cables in both configurations. The frequency converter of the machine is placed topside at the sending end of the cables in the first configuration and subsea at the receiving end in the second. The starting method is direct on-line starting in both cases. A summary of the motor start up analysis results is given in Table 5.3. The motor terminal voltage and speed of the motors for the two scenarios are both plotted in Figure 5.1 and the active and reactive power consumption of both cases in Figure 5.2.

Converter Location	Motor Voltage		Starting Current	Starting PF	Approx. Starting Time
	Min.	After			
Topside	0.695 p.u.	0.966 p.u.	5.900 kA	0.184	32.713 s
Subsea	0.873 p.u.	0.987 p.u.	8.065 kA	0.673	18.763 s

Table 5.3: Summary of Model D motor start up simulation.



(a)



(b)

Figure 5.1: Model D: Motor bus voltage (a) and motor speed (b) during start up.

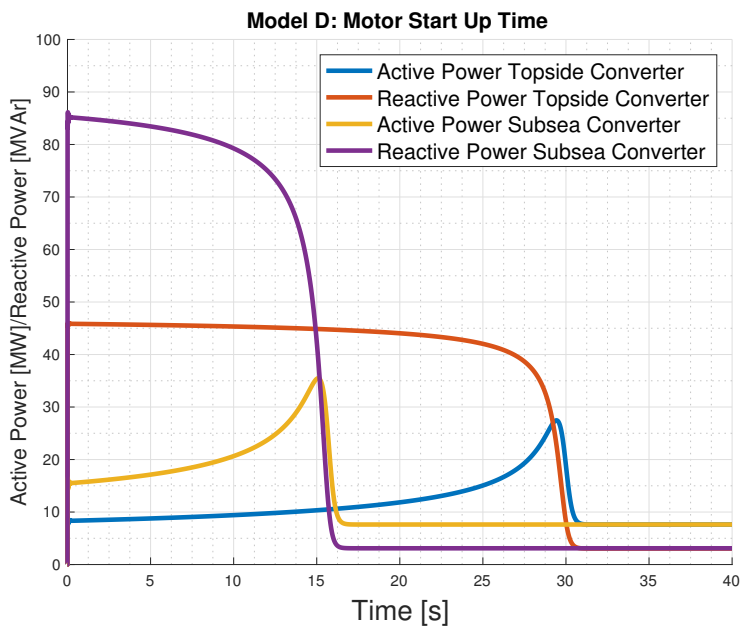


Figure 5.2: Active and reactive power consumption during star up for both converter configurations in Model D.

Figure 5.1a show that the start up time is approximately twice as long for configuration 1 (topside converter), compared to configuration 2 (subsea converter). In both configurations the machine starts successfully. However, as Figure 5.1b show, is the motor terminal voltage for configuration 1 at 0.7 p.u. during the entire start up, as opposed to configuration 2 where the voltage immediately drops to 0.95 p.u. and dips at 0.873 p.u. (when the motor reaches rated speed). This reduced voltage can be explained by studying the reactive power consumption presented in Figure 5.2. The reactive power consumed by the motor is supplied by the converter and thus limited to the capacity of the cable in configuration 1. For this configuration the power consumption is close to constant the first 15 seconds, and then slowly increasing (active power, decreasing reactive power) for the following ten seconds. This is because the cable has reached its current carrying limits (as described in Chapter 3.3), resulting in close to constant values as the motor is magnetized. This is verified by simulating an ideal cable (resistance and reactance equal to zero) for the topside converter configuration; the cable will have no voltage drop as there are no ohmic losses and the motor's need of reactive power is supplied through the cable without any constraints, thus starting the motor within 16 seconds. However, for the non-ideal cable, the starting current of 5.9 kA limits the power supply and extends the start up time of the motor.

For configuration 2 the situation is more identical to the example of with an ideal cable; as the simulated converter is ideal the reactive power required to magnetize the motor is delivered right away without any constraints, hence the high reactive power curve in Figure 5.2. This enables the motor to accelerate faster than in configuration 1. The active power is delivered from the topside bus so the voltage dip occurs as the active power consumption peaks and thus the loading of the cable is at its maximum. In addition to the faster start up time and higher voltage the starting PF is improved for configuration 2.

5.1.3 Model C Load Flow Analysis

A load flow analysis is also carried out for Model C. The subsea distribution station of the model is supplied with power through two identical cables in order to achieve a loading of the cables below 100 %. The cable size, loading and voltage drop is presented in Table 5.4.

Cable (XLPE-CU)	Loading	V_d
3×300 mm	78.67 %	4 %
3×300 mm	78.67 %	

Table 5.4: Model C load flow simulation cable size, loading and voltage drop.

The loading of the components in the model is similar to Model A and B, and the active power losses are very similar to Model B. The grid active power loss is 260 kW (3.2 %) and the reactive power loss is 310 kVAr. Model C has a somewhat high reactive power loss compared to Model B, thus the model has an external infeed of 8.16 MW and 5.20 MVar. The increased reactive power loss is expected as

the delivered power of each cable is above the surge impedance loading (described in Chapter 3.3) of the cables.

5.1.4 Simple Model Simulations Summary

The three simple model load flow simulations show that feeding each SPT component individually results in an unacceptable high active power loss, thus combining the power supply to each SPT is essential in order to reduce the distribution losses and voltage drop of the system. This is also a practical matter, as deployment, operation and recovery of a SPT would be more complicated with an increased number of umbilicals. A further discussion of the results is presented in Chapter 6. The PowerFactory load flow simulation models are depicted in Appendix E.

Based on the simulation results of the simple models Model B and Model C was further developed to Model 1-4 as both these system topologies were deemed to have potential for DSM power distribution.

5.2 Steady State Load Flow Analysis

The first simulation of Model 1-4 is a simple steady state load flow analysis. This is done in order to identify the power losses and voltage drop of the different system topologies. For all the models the SPTs are loaded at approximately 70 % of their total installed active power. This is done by loading the pump drive and mining tool at full load and adding 100 kW to a passive load for each machine. This loading is the same for all the models. In addition to this the SPTs in Model 1 and Model 2 are loaded with an extra passive load in order to take consideration of an extra reactive power requirement for the SPTs. This is further explained in Chapter 5.2.1. The loading of the TS components is the same for all the models. The SSLP pumps are loaded at 80 %, the DP 10 MW and 6.2 MVar (40 % of full load at 0.85 PF) and the passive load representing the ore dewatering plant, hotel loads and auxiliary systems is aggregated to 1.0 MW and 0.62 MVar (40 % of full load at 0.85 PF). The loading of the TS and SS components is summarized in Table 5.5. For all the simulations two of the three diesel-generator sets are running as this is sufficient to cover the presented power requirement.

The cables are dimensioned on the basis of these simulations. They are selected in order to be loaded between 60 - 70 % during the operation described above. The cables are selected from the PowerFactory-library and their values are compared to the selection of cables in [40] in order to assure that they are adequate. The technical data of all the selected cables are presented in Appendix G.

	Component	Active power	Reactive power	PF	Loading
TS	DP	10.0 MW	6.2 MVar	0.85	40 %
	Hotel & auxiliary	1.0 MW	620 kVar	0.85	
	SSLP pump	8.55 MW	3.58 MVar	0.92	78.98 %
AUX	Pump	800 kW	330 kVar	0.93	99.38 %
	Tool	800 kW	330 kVar	0.93	99.38 %
	Passive	200 kW	0 kVar		
BC	Pump	800 kW	330 kVar	0.93	99.38 %
	Tool	1300 kW	530 kVar	0.93	99.38 %
	Passive	200 kW	0 kVar		
CM	Pump	900 kW	370 kVar	0.93	99.38 %
	Tool	500 kW	180 kVar	0.94	98.09 %
	Passive	200 kW	0 kVar		
SUM		25.25 MW	12.47 MVar		

Table 5.5: Loading of SPT- and TS-components during steady state load flow analysis Model 1-4.

5.2.1 Model 1 and Model 2

The load flow analysis results of Model 1 and Model 2 gives the same indication as those of Model B and Model C; combining the power distribution decreases the transmission losses. The voltage drop V_d of the cables are approximately 4% for all cables in both models. This is an acceptable voltage drop, considering that none measures are done in order to minimize the voltage drop (e.g. increased transmission voltage, utilizing SVC or STATCOM). The power loss of the cables are 235 kW and 179 kW for Model 1 and Model 2 respectively. For Model B and C the power loss was approximately the same for both models, but for Model 2 the power loss is considerably lower compared to the power loss of Model 1. This is due to the cable dimensioning, as the cables in Model C are loaded at 80% apposed to Model 2 where they are loaded at 65%. The resulting cable size, loading, voltage drop, current and power loss of the Model 1 and Model 2 are presented in Table 5.6 and Table 5.7. In order to supply the subsea distribution station in Model 2 two cables are used. This is done in order to obtain a loading of 65%. The selected cables are two 3×185 mm cables. Since the cables are identical their loading, voltage drop V_d , current and power loss are the same. The data of all the selected cables are presented in Table G.1.

	Cable (XLPE-CU)				Power loss
	Cross section	Loading	V_d	Current	
AUX	3×95 mm	58.55 %	3.9 %	0.17 kA	68.87 kW
BC	3×120 mm	66.18 %	4.1 %	0.22 kA	90.01 kW
CM	3×70 mm	62.75 %	4.7 %	0.15 kA	75.80 kW

Table 5.6: Model 1: Load flow simulation cable size, loading, voltage drop, current and power loss.

A summary of the active, reactive and apparent power flow for Model 1 and Model 2 is presented in Table F.1 in Appendix F. As the simulated converters are assumed ideal there is no reactive power flow from the topside generation units to the subsea components as reactive power needed for the subsea motors is supplied directly from the inverter. To obtain a realistic approximation of the SPT reactive power consumption an extra passive load is added to each AC bus of the SPT in order to obtain a realistic cable dimensioning, assuming that the SPT in reality would consume some reactive power provided by the TS. In order to correct for this passive loads are added at the receiving end of the cables. The loads are assumed to draw the same amount of reactive power as the inverters deliver to the motors of the SPTs.

In both models the two running generators are identical in loading and operation. The current of each generator is 1.239 kA and the running diesel-generator sets are loaded at 83% in both models. The only difference in active power between the two models is a small increase in active power generation in Model 1 as the grid losses are 230 kW and 180 kW for Model 1 and Model 2 respectively. Model 1 has a reactive power generation somewhat lower than Model 2 due to the fact that

the line charging of the cables in Model 1 produces (almost) the exact amount of reactive power as the cables consume, and in Model 2 the line charging is close to negligible while the reactive power consumption is over twice as much as for Model 1. This is further discussed in Chapter 6.3. The PF of the generators are 0.90 for both models.

Cable (XLPE-CU)				
Cross section	Loading	V_d	Current	Power loss
3×185 mm	65.34 %	3.6 %	0.27 kA	89.28 kW
3×185 mm	65.34 %	3.6 %	0.27 kA	89.28 kW

Table 5.7: Model 2: Load flow simulation cable size, loading, voltage drop, current and power loss.

5.2.2 Model 3 and Model 4

The power loss of Model 3 is almost the same as the power loss of Model 1. This is expected as the voltages of the models are chosen in order for the models to be similar. The power loss of the SPT cables are somewhat different in the two models as their loading are different. For the DC distribution in Model 3 each SPT is supplied with active power through two cables as a bipolar DC-system is used. Four cables are used in Model 4, two for each polarity, in order to achieve a loading below 70 %. The cable size, loading, voltage drop, current and power loss for Model 3 is presented in Table 5.8 and for Model 4 in Table 5.8. N2YSY single core XLPE insulated copper cables are chosen from the PowerFactory library for both models. The technical specification of the cables are presented in Table G.2 in Appendix G.

		Cable (N2YSY-CU)				
		Cross section	Loading	V_d	Current	Power loss
AUX	Pos.	1×150 mm	69.60 %	4.4 %	0.29 kA	41.69 kW
	Neg.	1×150 mm	69.60 %		0.29 kA	41.69 kW
BC	Pos.	1×300 mm	62.38 %	2.7 %	0.36 kA	33.60 kW
	Neg.	1×300 mm	62.38 %		0.36 kA	33.60 kW
CM	Pos.	1×120 mm	67.91 %	4.8 %	0.25 kA	40.36 kW
	Neg.	1×120 mm	67.91 %		0.25 kA	40.36 kW

Table 5.8: Model 3: Load flow simulation cable size, loading, voltage drop, current and power loss.

		Cable (N2YSY-CU)				
		Cross section	Loading	V_d	Current	Power loss
Pos.	1	1 × 500 mm	64.58 %	1.8 %	0.44 kA	28.40 kW
	2	1 × 500 mm	64.58 %			
Neg.	1	1 × 500 mm	64.58 %	1.8 %	0.44 kA	28.40 kW
	2	1 × 500 mm	64.58 %			

Table 5.9: Model 4: Load flow simulation cable size, loading, voltage drop, current and power loss.

A summary of the active, reactive and apparent power flow for Model 3 and Model 4 is presented in Table F.2 in Appendix F. As both systems are DC systems there is no reactive power flow in the cables, hence no line charging or reactive power losses in the systems. As the subsea motors are supplied with reactive power from the converters in a DC system, no correction with passive loads (which was done for Model 1 and 2) is done for these models as all the reactive power consumption of the SPT must be delivered by components on the SPT. The two running generators are identical in loading and operation. The active power loss in Model 3 is 231 kW and in Model 4 it is 114 kW. As there is no reactive power loss in the cables the generator loading is a bit lower for Model 3 and Model 4, compared to Model 1 and Model 2. The loading of each generator is approximately 81 %. The current is 1.20 kA for both generators in both models. As the load flow analysis of Model A-C indicated is the active power loss lower for the combined distribution system lower for the combined distribution to the SDS compared to the individual SPT power supply.

5.3 Harmonics and Power Quality Analysis

Power quality is an important aspect for all power systems. As described in Chapter 3.1 there are international guidelines, standards and acceptance limits of allowable harmonic content in all power systems. Therefore, a power quality analysis is performed for Model 1-4. PowerFactory has a designated harmonic load flow analysis function which calculates the total harmonic distortion for all AC buses in the system. The simulation tool treats all harmonic sources in accordance with IEC 61000-3-6. This standard is not the same as [23] refers to when defining allowable harmonic distortion (i.e. IEC 61000-4-2), but the corresponding standard for requirements for the connection of distorting installations to MV, HV and EHV public power systems. Despite the difference, the simulation tool is deemed suitable for offshore power system harmonic analysis.

As all converters in the simulation model are modelled as ideal converters there will be no harmonic distortion in the system. Therefore, specified current harmonics are added to each converter in all the models. The current harmonics specifications are from the PowerFactory library harmonic injection spectrum '12-Pulse Bridge' (B12). The different magnitude of the current harmonics are presented in Figure 5.3. The injected harmonics are specified according to the fundamental current of the component.

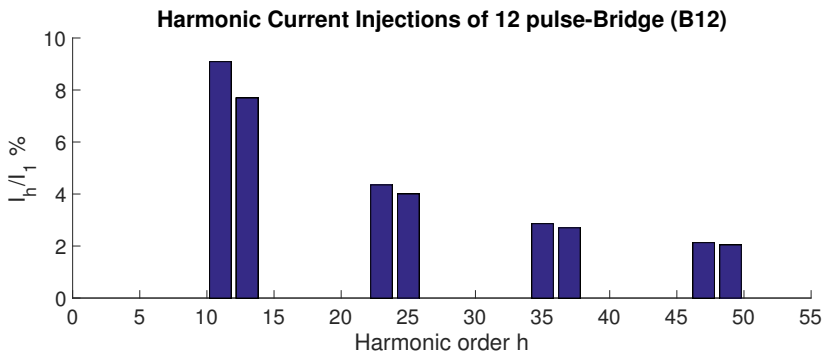


Figure 5.3: Harmonic current injected in relation to fundamental current I_h/I_1 .

As the harmonic representation is similar for all models it will be easy to differentiate the influence of the harmonic distortion on the different models. The simulation results are presented below and further discussed in Chapter 6.5.

5.3.1 Model 1

The first model to be analyzed is Model 1. The loading of the components is not changed from the load flow analysis in Chapter 5.2, which makes the PF and currents in the system unchanged. The results of the power quality simulation are given in Table 5.10. In addition, the maximum short circuit currents I_{SC} and load current I_1 of all the buses are given in the table. Using Table 3.1 and the ratio I_{SC}/I_1 the acceptable THD for each bus is found.

	AC bus	PSV	AUX	BC	CM
2 gen-sets	THD (%)	12.6	20.2	21.6	19.7
3 gen-sets		7.7	14.3	15.6	13.9
2 gen-sets	I_{SC} (kA)	22.042	4.263	4.918	3.359
3 gen-sets		30.24	4.414	5.143	3.436
Load current I_1 (kA)		2.478	0.17	0.22	0.15
Acceptable THD (%) (according to Table 3.1)					
2 gen-sets		5.0	8.0	8.0	8.0
3 gen-sets		5.0	8.0	8.0	8.0

Table 5.10: THD and I_{SC} for all AC buses in Model 1.

The THD in the system is at an unacceptable high level when two generators are running. For the PSV main AC bus the THD is 12.6%. According to Table 3.1 it should not be above 5%. As mentioned in Chapter 3.1.1, the limits in Table 3.1 are not specified for offshore power systems where, according to IEC 61000-2-4, the THD shall not exceed 8% [23]. Regardless of this, a THD of 12.6% is unacceptable and measures should be done in order to lower it. For the buses on the SPTs the THD is in the range of 19-22%. As the load current is relatively low for the SPTs the ratio I_{SC}/I_1 will allow a THD of 8% for these buses. The THD of 19-22% is therefore at an unacceptable high level. By increasing the number of generators in operation the THD can be lowered significantly. By running three generators the THD is lowered for all buses. By operating three generators the maximum short circuit current (of all buses) is increased and the loading of each generator is decreased to 55.5%. The THD of the topside bus is lowered to 7.7%, which is within the limit specified by IEC 61000-4-2. The THD of the SPT buses is lowered to 14.3%, 15.6% and 13.9% for the AUX, BC and CM respectively. This value is not acceptable and there will be a need for further improvement.

5.3.2 Model 2

For Model 2 the topside TS THD is somewhat higher than for Model 1. When powering the system with two generators the THD is 13.3% at the topside bus and 25.6% at the subsea distribution station. By running three generators the THD is decreased to 8.0% (topside) and 18.6% (subsea). For the TS is the THD is just at the acceptable limit, but the subsea distribution station will violate the 8% limit when the system is operated with both two and three generators. As for Model

1, the THD for the two buses, the short circuit current and acceptable THD (for operation of both two and three generators) are tabulated in Table 5.11.

	AC bus	PSV	Subsea
2 gen-sets	THD (%)	13.3	25.6
3 gen-sets		8.0	18.6
2 gen-sets	I_{SC} (kA)	22.042	9.748
3 gen-sets		30.24	10.919
Load current I_1 (kA)		2.481	0.548
Acceptable THD (%) (according to Table 3.1)			
2 gen-sets		5.0	5.0
3 gen-sets		5.0	5.0

Table 5.11: THD and I_{SC} for topside and subsea AC buses in Model 2.

As the table presents; the short circuit currents for the PSV are the same as for Model 1, which is as expected since the TS is unchanged. For the subsea distribution station is the ratio I_{SC}/I_1 just below 20 for both operating scenarios (17.8 when operating two generators and 19.9 when operating three) so the acceptable THD is limited to 5% according to Table 3.1. Accordingly, as for Model 1, measures should be done in order to lower the THD.

5.3.3 Model 3 and Model 4

For Model 3 and Model 4 the THD of the topside AC bus is within the acceptable limit of 8% specified in IEC 61000-4-2. The THD and short circuit currents are presented in Table 5.12. This result is as expected as there is no reactive power flow from the TS to the SS, and the only topside component which is not simplified to a passive load is the SSLP pump drive. This proves that utilizing DC distribution for DSM power supply is favourable regarding the effects of THD.

		Model 3	Model 4
2 gen-sets	THD (%)	6.6	6.5
3 gen-sets		5.0	4.9
2 gen-sets	I_{SC} (kA)	22.042	
3 gen-sets		30.24	
Load current I_1 (kA)		2.408	
Acceptable THD (%) (according to Table 3.1)			
2 gen-sets		5.0	
3 gen-sets		5.0	

Table 5.12: THD and I_{SC} for the topside AC bus (PSV) in Model 3 and Model 4.

5.4 BC Mining Tool Motor Start Up

A motor start up simulation is the last simulation. This simulation is chosen in order to investigate the affects of starting a large motor in the system. The simulation is performed on Model 1 and Model 2. The machine of the BC mining tool is chosen to be started as this is the largest subsea motor in the system. In addition to the start up results of the machine, the voltages at the other buses are studied in order to study the influence of the motor start up.

5.4.1 Motor Buses During Start Up

In the simulation the other motors in the system are all running. All the components are loaded as specified in Table 5.5. Direct on-line starting is used, and the motor is successfully started in both models. A summary of the motor start up is given in Table 5.13.

Model	Motor Bus Voltage		Starting Current	Starting PF	Approx. Starting Time
	Min.	After			
1	0.877 p.u.	0.955 p.u.	1,330 kA	0.675	21.163 s
2	0.934 p.u.	0.963 p.u.	1.366 kA	0.675	17.763 s

Table 5.13: Summary of BC mining tool motor start up.

The starting current and PF are identical for the two models. This is to be expected as they are fed by the exact same type of converter (with identical values) in both models. The start up time is shorter for Model 2; approximately 18 seconds, as opposed to 21 seconds for Model 1. The voltage drop is also larger for Model 1. For the AC bus of the BC in Model 1 the minimum voltage during start up is 0.877 p.u. The corresponding value for the SDS AC bus in Model 2 is 0.934 p.u. The voltage drop of Model 1 is greater as this bus has fewer components connected to it, which makes it more sensitive to load variations. The SDS in Model 2 has all the SS electrical components connected to it and is therefore more resistant to load variation, and thus the fluctuation in voltage is lower for this bus. The voltage curves of the two motors are both shown in Figure 5.4. As the figure shows; the voltage curves of the two motors are very similar. Once the motor is started the BC AC bus of Model 1 has a drop in the voltage from 0.978 p.u. to 0.937 p.u. For Model 2 is the voltage drop from 0.971 p.u. to 0.955 p.u. When the motor start up is complete, the BC AC bus voltage will stabilize at 0.955 in Model 1 and at 0.963 for the SDS AC bus in Model 2.

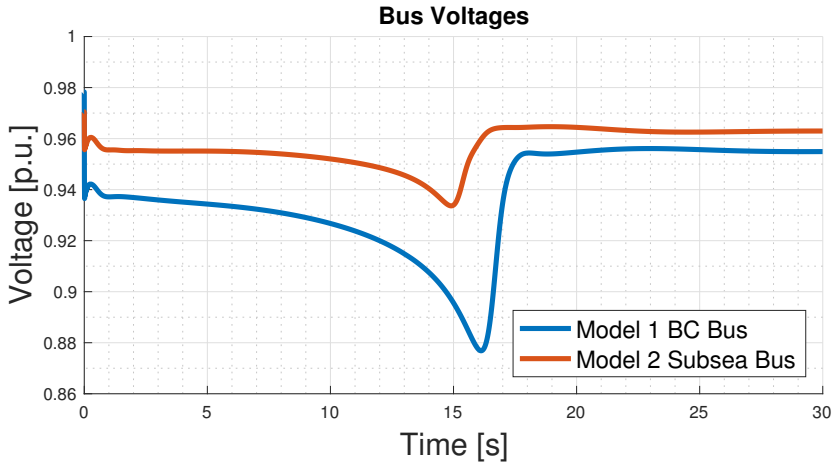
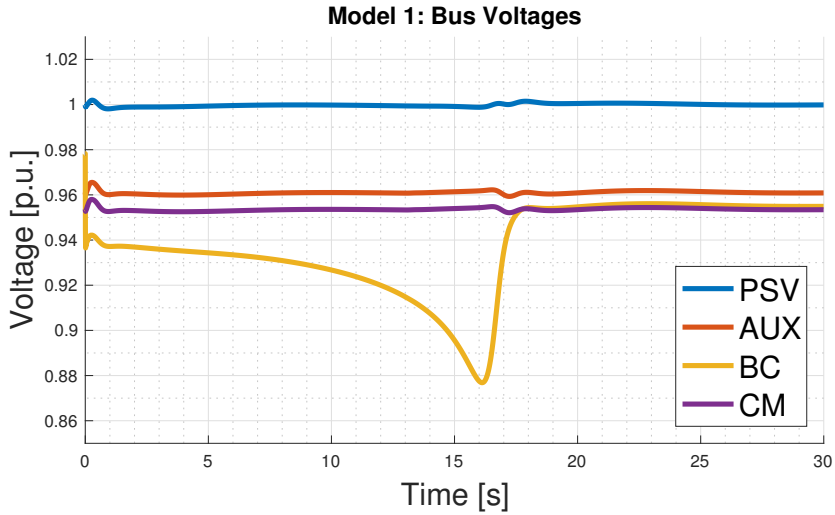


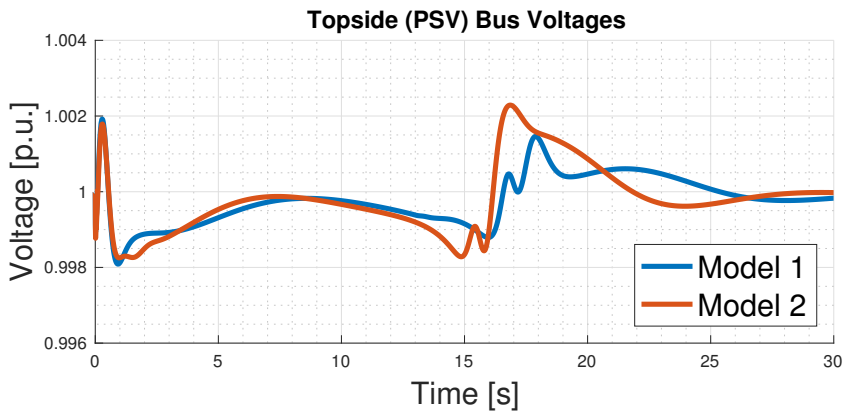
Figure 5.4: Motor bus voltage during start up of the BC mining tool for Model 1 and 2.

5.4.2 Influence on Other Buses

As the BC mining tool is started the other buses of the system will be affected. The start up of the large motor will however have a minimal influence on the operation of the other buses. The voltage of all the AC buses in Model 1 are depicted in Figure 5.5a. As the figure shows there is some flicker at the voltages of the PSV, AUX and CM buses. The voltages at the topside PSV AC bus for both models are shown in Figure 5.5b. These voltage fluctuations are within $\pm 0.4\%$, i.e. they are negligible. The largest influence on other equipment will be to the components connected to the same bus as the BC mining tool. For Model 1 this is the BC pump drive and other auxiliary loads. These components will need to be able to tolerate the voltage drop to 0.877 p.u. For Model 2 all the SS components will be affected as they are all connected to the same bus. Although the voltage drop is lower for Model 2, measures should be done in order to minimize the voltage drop during start up as all SS components are connected to the same bus and a malfunction at the SDS would disable the entire production system.



(a) Model 1 bus voltages during start up of the BC mining tool.



(b) Topside bus voltages (PSV) during start up of the BC mining tool for Model 1 and 2.

Figure 5.5: Model 1 bus voltages (a) and topside bus voltages (PSV) (b) during start up of the BC mining tool.

Chapter 6

Discussion

In this chapter the result presented in Chapter 5 are discussed. Based on the results the different models (their system topologies) are evaluated for powering a DSM production system.

6.1 Simple Models

The simulations of the simple models excludes the system topology of Model A as a possibility for DSM application, due to the extensive power loss of the system. In addition to this, the seemingly advantage of placing the converters topside proves to be inefficient for the operation of the machines (e.g. during start-up). Topside converters will also occupy scarce place on board the PSV.

The load flow simulation of Model B and C shows that the two system topologies have an active power loss of 270 kW (Model B) and 260 kW (Model C). This power loss is more acceptable (3.2- 3.3%), but the system topologies require to install subsea distribution stations, either on each SPT fed individually or one common installation. Since the simulation results of Model D proved that locating the converters at the motor terminal improves the motor performance tremendously, the system topologies of Model B and Model C was chosen to be further investigated, with both AC and DC distribution.

6.2 Model Structure and Cost Comparison

The different system topologies will have a different number of umbilicals, cables and converters. Accordingly, they will have different investment and operational costs. As there are no 'off-the-shelf' components for such advance and new technology as DSM, combined with corporate restraint of publishing such information, it is difficult to estimate the costs of the different topologies. However, by comparing the number of different components and their power rating an indication of the investment cost may be obtained.

6.2.1 Individual SPT Power Distribution (Model 1 and Model 3)

The system topology of Model 1 and Model 3 has many advantages and is natural to investigate as it is the chosen topology of the Nautilus Minerals SPS. Since the SPTs has individual power supply they can be operated independent of each other and their operations does not influence each other (other than occupy generator capacity). This increases the total redundancy of the mining operations, as in the event of a breakdown for one of the SPTs the two other can continue operation. In addition to this is the number of subsea cables is reduced to three (compared to Model A), which reduces the investment cost of expensive armoured subsea cables, and also reduces the total weight of the system. It is assumed that in both models all the cables (power, communication, sensors etc.) of the SPTs are bundled into one umbilical. The launch and recovery will also be simplified (compared to Model A) as the handling of the SPTs will be less challenging when only one umbilical per SPT is used.

Another result of only one cable powering the SPT is that the frequency converters of each motor must be installed on the SPT in order to control the speed and torque of the machine. This will increase the cost of the system as the converters (as all other SPT components) must be designed for subsea operation in an ambient pressure of approximately 350 bar. For Model 3 will only the inverter part of the motor converter be installed on the SPT, as it has DC-distribution. This will be the case for Model 4 as well. However, limited space on board the TS will be available for other application, such as ore- and fuel-storage which is an important feature of the production system as this will reduce the need for fuel replenishment at sea and increase the ore storage capacity. Another consequence of installing the converters on the SPTs is the increased weight of the SPTs. This may not be a drawback as the SPTs will require some weight in order to penetrate the seabed with its cutter head [41].

6.2.2 Combined Subsea Power Distribution (Model 2 And Model 4)

The system topology of Model 2 and Model 4 will most likely have a higher production cost than Model 1 and Model 3 due to the subsea distribution station. The distribution station may be as large in size and weight as the SPTs and a storage and handling system similar to that of the SPTs could be used for the SDS.

There are several advantages of this system topology. As the SPTs are powered from the SDS, instead of the TS, the SPTs can be designed in a new way, e.g. more of the electric components may be installed in the SDS if increased power capacity of the SPTs is needed for new DSM operations without increasing the weight of the SPT. Higher power and voltage ratings (compared to the Nautilus Minerals System) will also be required as the SDS is to power the entire SS. For DSM in deeper waters it is possible that the UTS will be re-designed, e.g. to be powered by electricity from the seabed. This will increase the power demand at the seabed considerably.

Combined with an increased power demand for DSM in deeper waters (e.g. the Norwegian Sea) using a SDS could prove to be favourable as the SDS could be powered by a lower number of umbilicals at a higher voltage level. By increasing the number of umbilicals powering the SDS (to more than one) the redundancy of the system will be increased. In the event of a malfunction on one of the umbilicals the other can be loaded heavier in order to continue operations or perform a controlled production stop. By installing an increased number of umbilicals, combined with fault monitoring systems, the seafloor production may even be optimized to continue during planned maintenance outages [42]. This will of course require all umbilicals to be equipped with wet-mateable connectors at the SDS cable terminations (as described in [31]) in order to remove them without affecting the other components during operation. This will also apply to the SPTs if they are to be removed separately from the system during operation of the other system components.

With respect to future power solutions for DSM application, the system topology will enable the possible implementation of alternative subsea energy sources. As the DSM process may take place near active smokers emitting fluids at high temperatures, harvesting geothermal energy may be a possibility to increase the implementation of renewable energy. The SDS will ease the integration of the equipment necessary to implement such alternative energy resources as it will be located on the seafloor.

6.2.3 Converters

Model 1 will need six AC/AC converters installed on the SPTs in order to control the cutter head and the pump drive of the machines. This is a simplification as the SPTs in reality will have more motors, e.g. the track drive systems and boom cutter hydraulics. As this simplification is done for all the models it will not affect the comparison of the models. For all models the converters must be rated to match the installed effect of the component(s) it is supplying. The different type of converters needed by the different models are summarized in Table 6.1. Model 2 will have the same type and number of converters as Model 1. Model 2 will however have the possibility of installing the converters in the subsea distribution station and thus differ from Model 1.

Model 3 and Model 4 will only need the DC/AC inverter located on subsea as the models have DC distribution to the subsea components. Although, this may not result in a lower cost as the DC distribution is a less developed technology. The number of components is still reduced and thus may be favourable with respect to size and weight of the converters necessary on the SPTs or in the SDS.

Model Number	Converter Type				Power Rating
	1	2	3	4	
AUX Centrifugal Pump	AC/AC		DC/AC		800 kW
AUX Mining Tool	AC/AC		DC/AC		800 kW
BC Centrifugal Pump	AC/AC		DC/AC		800 kW
BC Mining Tool	AC/AC		DC/AC		1,300 kW
CM Centrifugal Pump	AC/AC		DC/AC		900 kW
CM Mining Tool	AC/AC		DC/AC		500 kW
AUX Topside	-	-	AC/DC	-	1600 kW
BC Topside	-	-	AC/DC	-	2100 kW
CM Topside	-	-	AC/DC	-	1400 kW
Topside	-	-	-	AC/DC	5100 kW

Table 6.1: Converter requirement for all models.

6.3 AC Distribution

The power flow analysis of the models gives an indication of the different system topologies efficiency. Of the two AC models, Model 2 is the one with the lowest power loss. When operating the DSM electric power system at 6.6 kV the power loss is 56 kW lower for Model 2 than Model 1. The difference is marginal, but when operating the system this small difference may result in a lower operation cost over time. It is important to notice that the cables from the SDS to the SPTs are neglected in the simulations, and they will increase the losses. This loss will however be very small compared to the overall losses of the system. The voltage drop of the different cables in the two models are quite similar as they are in the range of 3.6-4.7%. The lowest voltage drop occur in Model 2, which implies that this system topology will be the least exposed to wear and tear in the insulation of the umbilicals of the two AC models.

By using Equation 3.24 and the data given in Appendix G the surge impedance loading of the cables used for AC distribution is calculated. The values are presented in Table 6.2.

Type	XLPE-CU			
Cross section	3×70 mm ²	3×95 mm ²	3×120 mm ²	3×185 mm ²
P_{SIL}	1338 kW	1466 kW	1551 kW	1817 kW

Table 6.2: P_{SIL} of the cables selected for AC distribution.

As the table shows is the surge impedance loading of each cable lower than the power consumption of the SPTs (presented in Table 5.5), which means that all the cables in Model 1 and Model 2 will be net consumers of reactive power. This differs from the statement in Chapter 3.3 that subsea cables usually are reactive power producers. This is due to the (relative) short distance of the cables in the DSM system. For Model 1 the reactive power consumption is almost cancelled by the line charging, but for Model 2 the reactive grid losses are greater than the line charging, resulting in a net consumption of reactive power. For Model 2 will it be natural to add a transformer in order to increase the transmission voltage as the SDS will power all SPTs. By installing a transformer, a galvanic isolation will be provided between the TS and SS. A higher distribution voltage will increase the production of reactive power (shown by Equation 3.21) and the ohmic losses in the cable will be further reduced as the current in the cable will decrease. However, the weight and cost of the equipment will consequently increase due to the increased number of components and the thicker insulation needed for the higher voltage rating of the cable.

As mentioned will it be possible to operate the system of Model 2 at a lower power loading in case of a malfunction on one of the two umbilicals. As the cables are dimensioned to be loaded at 60-70% at nominal operation of the SPTs, there is a possibility of utilizing the extra capacity of the cable for emergency operation, and thus loading the cable more. If one of the umbilicals in Model 2 is out of operation, the remaining cable will be loaded at 135% when the SS components are loaded as

presented in Table 5.5. By shutting down the mining tools of the SPTs the loading of the one cable is reduced to 80%. At this loading the production system will be able to perform a controlled shut down of the system, e.g. running the pumps in order to remove the last ore from the system, and then operate the track drive systems if a relocation of the SPTs is necessary before recovery.

6.4 DC Distribution

As for the AC distribution systems, is it the combined distribution to the SDS that has the lowest power loss of the two DC distribution systems. The power loss is 50 % lower for Model 4 (114kW) compared to Model 3 (231 kW). Despite the lower power loss of the distribution system is it important to emphasize that the combined distribution system will have a larger investment cost and that the umbilicals from the SDS to the SPTs are neglected, thus a marginal increase in distribution losses is to be expected for the combined distribution alternative.

Compared to the AC systems, the DC distribution systems will have lower power losses. For the individual SPT power distribution the losses are approximately the same (235 kW for AC, 231 kW for DC), but for the combined distribution to the SDS the losses for the ± 3 kV DC model are as low as 114 kW. For the corresponding 6.6 kV AC topology the losses are 178 kW.

In the simulation models the DC distribution voltage is ± 3 kV. For a TS with an AC system of 6.6 kV it will be necessary to step down the voltage in order to obtain this DC voltage (when using passive rectification, therefore voltage source converter would be utilized). Therefor, it will be more natural to use a higher DC voltage which will lower the distribution losses even further. A higher voltage level will however be challenging for the DC systems as the development of system components, such as MVDC voltage source converters and circuit breakers, are still not at a level which makes it commercially available [43]. Despite the lack of MVDC components, DC distribution for ship applications is emerging rapidly. There are several benefits of DC power distribution on ships, e.g. it will be possible to operate the generators more efficiently (consequently reducing fuel consumption, emissions and maintenance needs), DC components will require less space and it will be easier to implement (renewable) alternative energy resources [44].

6.5 Reducing Harmonics

Another aspect of the AC systems is the influence of THD. Once again it is important to specify that as most of the TS components are simulated as passive loads they do not contribute to the THD of the topside AC bus, which will be the case for the actual DSM power system. However, as this is similar for all models the comparison of the system topologies in relation to each other will be adequate when evaluating the system topologies content of THD.

The values of THD in Model 1 (presented in Table 5.10) shows that an unacceptable high amount of THD is present in the system during nominal operation (with both two and three generators running). The THD at the TS is reduced to an acceptable limit by running three generators, but the SPTs AC buses are still violating the limits given by [23] and IEC 61000-4-2. By adding a filter to the system, the THD can be limited to correspond to the limits given in Table 3.1. For Model 1 a simulation with a filter connected to the topside AC bus is performed. The filter connected to the TS is a capacitive shunt filter. The capacitance of the filter is $70.736 \mu\text{F}$ and has a rated reactive power of 960 kVAr. When two generators are running the filter reduces the THD of the subsea SPT buses to 5.2%, 6.5% and 4.9% for the AUX, BC and CM respectively. The THD at the main bus is at 0.5%, almost completely eliminated. The filter draws a total RMS current (as specified in Equation 3.10) of 132.2 A. The fundamental frequency rms current is 101.6 A and the harmonic RMS current is 84.55 A. The harmonic currents absorbed by the filter are tabulated in Table 6.3.

Harmonic order h	Frequency f_h (Hz)	Capacitor current (A)
1	60	101.61
11	660	56.56
13	780	44.65
23	1380	23.94
25	1500	22.13
35	2100	16.59
37	2220	15.91
47	2820	13.65
49	2940	13.37

Table 6.3: Harmonic currents absorbed by the filter.

This proves that measures can be done in order to reduce the THD. For Model 2 will it be natural (and most necessary) to install an active filter in the SDS since this component will be very exposed to harmonic distortion as all the components of the SS will be connected to this unit. This is proven by the power quality simulation of Model 2, presented in Chapter 5.3.2, as the THD for the subsea AC bus is as high as 25.6% and 18.6%, for system operation with two and three generators respectively.

For the two models with DC distribution the THD at the topside AC bus is within the limits of [23]. This is as expected due to the simplifications of the TS. However, the simulations show that using DC distribution to the seafloor components will give significant advantages for the power quality of the TS. Since THD will not be an issue for a complete DC distribution system, there are several different recommendations for DC ship distributions that should be applicable for DSM DC power distribution. Reference [38] describes characteristics such as voltage tolerances, withstand voltages, rated currents, duration of short-time withstand currents, grounding options galvanic isolation and so on. All of these (and many more) are important design aspects of a DC distribution system.

6.6 Voltage Fluctuations

The motor start up simulation of the BC mining tool proves a difference between the system topologies of Model 1 and Model 2. The voltage drop is greatest in Model 1, but more components are affected in Model 2 due to the common subsea AC bus in the SDS. Reference [1] defines a typical voltage tolerance limit for offshore power systems of $\pm 15\%$ during transient events and $\pm 5\%$ during steady state operations. None of these limits are violated during the start up of the BC mining tool. However, both the motor start up simulation and the load flow analysis (presented in Chapter 5.2) shows that the voltage at the subsea buses in Model 1, 2 and 3 are very close to violating the 5% steady state operation limit. Accordingly, the subsea buses should be equipped with voltage stabilizing equipment or filters in order to improve the voltage profiles of the buses. Another solution is to increase the transmission voltage as this will decrease the voltage drop in the cables, thus improving the voltage at the subsea buses.

Chapter 7

Conclusion

By studying different proposed system designs and R&D within the field of DSM, this thesis has proposed four different system topologies for an electrical power system designed to power a DSM production system for operation in the Norwegian Sea. As DSM is a new and growing industry the available publications and research within the subject is relatively scarce. Most of the published information is non-independent research from industry actors, and thus restricted as the companies have confidentiality agreements regarding their research and system concepts. The investigated research of both the vertical miner developed by Technip and BAUER and Nautilus Minerals' Solwara 1 Project have a lot in common, and it is therefore assumed that the power consumption and structure of DSM components based on this information is representative for DSM operations.

Based on the information presented in Chapter 2, four simple models were developed in the simulation software PowerFactory. These models provided results that led to the further development of the models presented in [1]. These models were developed to Model 1-4. The simulation models are simplified to such extent that they do not provide a realistic representation of the entire electric power system of a DSM production system. However, for the purpose of this thesis, the modelling of the electric power system is satisfactory. The representation of the components of the SPTs is adequate to simulate the behaviour of the SPTs in order to investigate the different AC and DC power distribution alternatives at a preliminary state.

For DSM operation in the Norwegian Sea an electrical power system with a centralized subsea distribution station is recommended. This system topology will have a significant lower power loss compared to the individual SPT distribution alternative, as proven by the simulations in Chapter 5. In addition, it will be natural to increase the transmission voltage as the power consumption of a DSM production system will increase when it is to operate at greater depths. By combining the power distribution at a higher voltage the distribution losses will be lowered even further. The influence of harmonic content and voltage deviation will be of great importance in a SDS. As the SDS will (most likely) have different switchboards and an advanced physical structure, the implementation of filters, provision of reserve energy and voltage and frequency stabilization equipment should be prioritized when designing the SDS.

For operations at depths beyond that of the Solwara 1 Project the UTS will most likely be redesigned to be electrically fed from the seabed. This increase in

required power at the seabed would make the combined distribution to a SDS even more reasonable, both with respect to the number of components (as the subsea riser pump would require a designated cable and distribution unit similar to the SPTs), active power loss and the overall cost of the system.

The downside of an electrical power system powering a SDS is the increased cost of such a system. Advanced economical analysis will be necessary to calculate a break-even operational depth of which the investment- and operational costs of a individual SPT distribution system will become greater than those of a combined distribution to a SDS. However, as the Solwara 1 Project will operate at 1,700 m depth it is logical to assume that the individual SPT power supply will be financially reasonable up to (at least) this depth.

Simultaneously as DSM emerges as a new industry, DC distribution technology is increasing within offshore applications. The advantages of a DC DSM production system, such as smaller, fewer and lighter converters, increased system redundancy and lower maintenance costs, will make DC distribution preferable in the future. However, AC technology is currently dominating the offshore industry as DC technology is not commercially competitive to the maturity of offshore AC technology.

A possible continuation of this thesis would be to investigate the behaviour of the proposed system topology for different operational scenarios. A further development of the PowerFactory models would also be natural, simulating the TS more accurately.

References

- [1] F. Williksen. An introduction to electric power system in deep sea mining applications. *Specialization Project*, December 2016. Unpublished.
- [2] E. Frimanslund. Feasibility of deep-sea mining operation within norwegian jurisdiction. Master's thesis, NTNU, June 2016.
- [3] M. D. Hannington, J. Jamieson, and S. Petersen. Seafloor massive sulfide deposits: Continuing efforts toward a global estimate of seafloor massive sulfides. In *OCEANS 2015 - Genova*, pages 1–3, May 2015.
- [4] R.E. Boschen, A.A. Rowden, M.R. Clark, and J.P.A. Gardner. Mining of deep-sea seafloor massive sulfides: A review of the deposits, their benthic communities, impacts from mining, regulatory frameworks and management strategies. *Ocean & Coastal Management*, 84:54 – 67, 2013.
- [5] Rolf B. Pedersen, Hans Tore Rapp, Ingunn H. Thorseth, Marvin D. Lilley, Fernando J. A. S. Barriga, T. Baumberger, and *et al.* Discovery of a black smoker vent field and vent fauna at the Arctic Mid-Ocean Ridge. *Nature Communications*, 1, 2010.
- [6] M. Figoni and S. Chand. A classification society's experience with subsea mining. In *International Ocean and Polar Engineering Conference*. International Society of Offshore and Polar Engineers (ISOPE), June 2014.
- [7] Johann Rongau, Giovanni Spagnoli, and Benoit Waquet. Abyss miner: Design of a deep-sea vertical continuous excavator. In *MARTEC Brokerage event, Paris*. Technip and Bauer Maschinen, February 2013.
- [8] G. Spagnoli, S. A. Miedema, C. Herrmann, J. Rongau, L. Weixler, and J. Denege. Preliminary design of a trench cutter system for deep-sea mining applications under hyperbaric conditions. *IEEE Journal of Oceanic Engineering*, 41(4):930–943, Oct 2016.
- [9] Stefan K. Schwank. Cutter mining: Cross-over technology from civil engineering. In *Third International Future Mining Conference*. BAUER Maschinen GmbH, Germany, November 2015.
- [10] P. Jankowski, E. Heymann, P. Chwastiak, A. See, P. Munro, and I. Lipton. Offshore production system definition and cost study. *SRK Project NAT005*, 2010. SRK Consulting.

- [11] G.R. Jones, A.E. Inglis, A.P. O’sullivan, M. Howitt, G.M. Smith, R.G. Berndt, D.H. Jaffers, and N.W. Ridley. Method and apparatus for auxilary seafloor mining, April 24 2013. EP Patent App. EP20,110,794,958.
- [12] G.R. Jones, A.E. Inglis, A.P. O’sullivan, M. Howitt, G. Smith, R.G. Berndt, D.H. Jaffers, N.W. Ridley, and I. Maskell. Method and apparatus for bulk seafloor mining, November 14 2013. US Patent App. 13/805,188.
- [13] R.A. Judge and A. Yu. Subsea slurry lift pump for deepsea mining. In *OMAE2010-205*. International Conference on Ocean, Offshore and Arctic Engineering, June 2010.
- [14] S.A. Schulte. Vertical transport methods in deep sea mining. Master’s thesis, TU Delft, June 2013.
- [15] A. Yu and P. Espinasse. Extending deepwater technology to seafloor mining. In *OTC 19912*. Offshore Technology Conference, May 2009.
- [16] J. Bialek, J. Bumby, and J. Machowski. *Power System Dynamics: Stability and Control*. John Wiley & Sons, LTD, West Sussex, PO19 8SQ, United Kingdom, second edition, 2008.
- [17] N. Mohan, T. Undeland, and W. Robbins. *Power Electronics: converters, applications and designs*. John Wiley & Sons, Inc, Hoboken, US, 2003.
- [18] I. Pierre, M. Zoglauer, D. Travers, K. Imhof, D. Chury, J. L. Harris, and et al. Security of electricity supply - Roles, responsibilities and experiences within the EU. *Report of Working Group on Security of Electricity Supply of the Union of the Electricity Industry - EURELECTRIC*, 2006-180-0001, Jan 2006.
- [19] K. Rudion, Z. A. Styczynski, A. G. Orths, M. Powalko, and H. Abildgaard. Reliability investigations for a dc offshore power system. In *2013 IEEE Power Energy Society General Meeting*, pages 1–5, July 2013.
- [20] Ian Charles Evans and Ras Al Khaimah. The importance of acceptable electrical power quality to the drilling industry worldwide. *Society of Petroleum Engineers*, SPE-166773-MS, Oct 2013.
- [21] J. F. Manwell, J. G. McGowan, and A. L. Rogers. *Electrical Aspects of Wind Turbines*, pages 205–256. John Wiley & Sons, Ltd, 2009.
- [22] IEEE recommended practice and requirements for harmonic control in electric power systems. *IEEE Std 519-2014 (Revision of IEEE Std 519-1992)*, pages 1–29, June 2014.
- [23] DET NORSKE VERITAS. Electrical installations. *DNV-OS-D201*, April 2011.
- [24] T. S. Haugan and E. Tedeschi. Reactive and harmonic compensation using the conservative power theory. In *2015 Tenth International Conference on Ecological Vehicles and Renewable Energies (EVER)*, pages 1–8, March 2015.

- [25] F.S. Williksen. Electrical power system in deep sea mining application. 2016. Student Paper ELK23-Power Electronics in Future Power Systems, NTNU - Unpublished.
- [26] Elisabetta Tedeschi. ELK23-Power Electronics in Future Power Systems. Lecture slides, August 29, 2016.
- [27] Elisabetta Tedeschi. ELK23-Power Electronics in Future Power Systems. Lecture slides, October 11, 2016.
- [28] M. Hedayati and H. Oraee. Assessment study of shunt facts devices for improving dynamic behavior of induction motors. In *2005 International Conference on Power Electronics and Drives Systems*, volume 2, pages 1352–1355, Nov 2005.
- [29] P. Vuorenpää and P. Järventausta. Enhancing the grid compliance of wind farms by means of hybrid svc. In *PowerTech, 2011 IEEE Trondheim*, pages 1–8, June 2011.
- [30] A. Nysveen. Start-up of motor drives with long cable and step-up transformer. TET4200 Marine and Offshore Power Systems, Department of Electric Power Engineering, NTNU. Lecture slides, April 8, 2016.
- [31] A. Nysveen. *TET4200 Maritime and Offshore Power Systems*. NTNU, Department of Electrical Power Engineering, Trondheim, Norway, 2016.
- [32] T. Toftveaag. Offshore HVAC Electric Power Transmission Systems – an Example. ELK-12 Wind power in electric power systems, Department of Electric Power Engineering, NTNU. Lecture slides, September 15, 2016.
- [33] E. Ildstad. *TET4160 Insulating Materials for High Voltage Applications*. Trondheim, Norway, August 2015.
- [34] L. Colla. Technical issues on the integration of long distance ac cables in hv and ehv networks. In *IEEE PES Insulated Conductors Committee Spring 2012 meeting*, Seattle, March 2012.
- [35] Benoit Waquet, Donald Faulds, and Ali Benbia. Understanding the effects of deep-sea conditions on seafloor massive sulfide deposits crushing process. January 2011.
- [36] B. Zahedi and L. E. Norum. Modeling and simulation of all-electric ships with low-voltage dc hybrid power systems. *IEEE Transactions on Power Electronics*, 28(10):4525–4537, Oct 2013.
- [37] R. Nilsen and I. Sorfonn. Hybrid power generation systems. In *2009 13th European Conference on Power Electronics and Applications*, pages 1–9, Sept 2009.
- [38] IEEE recommended practice for 1 kV to 35 kV medium-voltage DC power systems on ships. *IEEE Std 1709-2010*, pages 1–54, Nov 2010.

- [39] ABB. High voltage induction motors for chemical, oil and gas. *9AKK104340 EN*, Feb 2008.
- [40] Nexans Energy Networks. 6-36 kV Medium Voltage Underground Power Cables - XLPE insulated cables.
- [41] Giovanni Spagnoli, Arthur Bi, and Leonhard Weixler. Trench cutter case histories and their possible application for offshore piles as relieve drilling. *Geotechnical and Geological Engineering*, 32(3):713–724, 2014.
- [42] M. Seltzer-Grant, P. McKeever, L. Renforth, and S. Djokic. Combined power quality and condition monitoring of offshore networks. In *22nd International Conference and Exhibition on Electricity Distribution (CIRED 2013)*, pages 1–4, June 2013.
- [43] U. Javaid, D. Dujić, and W. van der Merwe. Mvdc marine electrical distribution: Are we ready? In *IECON 2015 - 41st Annual Conference of the IEEE Industrial Electronics Society*, pages 000823–000828, Nov 2015.
- [44] J. Lindtjørn J. F. Hansen and K. Vanska. Onboard dc grid for enhanced dp operation in ships. MTS Dynamic Positioning Conference, October 2011.
- [45] Phil Jankowski. Technical report 2011 PNG, Tonga, Fiji, Solomon Islands, New Zealand, Vanuatu and the ISA. *NI 43-101*, 2012. SRK Consulting.
- [46] J. Parianos. General update April 2016. *Nautilus Minerals*, 2016.

Appendix A

Growth stages of SMS deposits

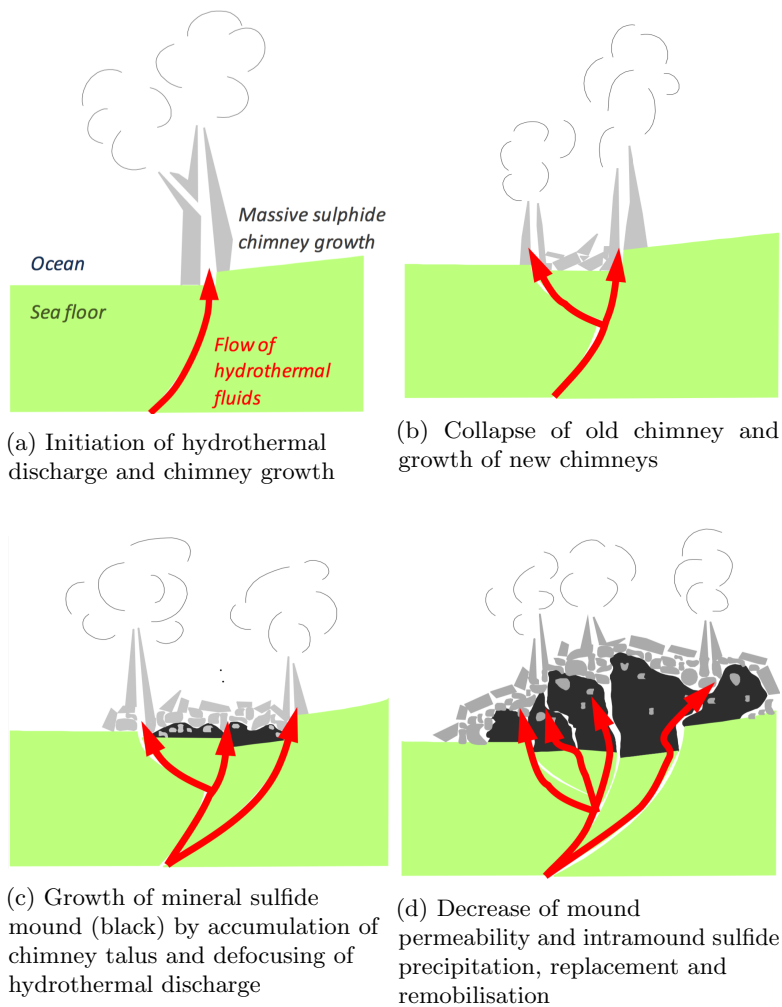


Figure A.1: Schematic diagram showing hypothesis for the development of SMS mounds on the seafloor [45, Figure 7-4, p. 60].

Appendix B

Estimation of SPT installed pump effect

The SPT installed pump effect is based on simple calculations of the relations between hydrostatic pressure, volumetric flow rate and required power. The calculations are based on parameters from [2, 10, 13].

The hydrostatic pressure of a given column of liquid, assuming the liquid is incompressible (i.e. having a constant density throughout the liquid), is given as:

$$p = \rho gh \quad (\text{B.1})$$

where p is the hydrostatic pressure (in Pascal), ρ is the fluid density (in kg/m^3), g is the gravitational acceleration (m/s^2) and h is the height difference between the highest and lowest point of the fluid (in m). By multiplying the hydrostatic pressure p by the required volumetric flow rate Q (in m^3/s) one obtains the power P required to lift the fluid.

$$P = pQ = \rho ghQ \quad (\text{B.2})$$

In order to approximate the power loss in the riser transfer pipe from the CM to the SSLP the known parameters of the UTS are used. According to [15], the total power consumption for the lift operation is <6.0 MW for 2,500 m and <4.0 MW for 1,700 m. However, the total installed power of the pumps delivering the pressurized sea water to the SSLP is 7.2 MW (assuming they are loaded at 100%). This implies an efficiency of 83.33 % for the system.

Solving Equation B.2 for Q gives a volumetric flow rate of approximately $0.186 \text{ m}^3/\text{s}$. The values used are:

$$\begin{aligned} \rho &= (3.3 \times 12\% + 1.03 \times 88\%) \times 1000 \text{ kg/m}^3 = 1302.4 \text{ kg/m}^3 \\ g &\approx 10 \text{ m/s}^2 \end{aligned}$$

which for $P = 4.0$ MW and $h = 1,700$ m gives $Q = 0.1844 \text{ m}^3/\text{s}$

and for $P = 6.0$ MW and $h = 2,500$ m, $Q = 0.1881 \text{ m}^3/\text{s}$.

Assuming that the SPTs are required to have (at least) the same flow rate as the UTS (in order to not limit the production rate) and that the SSLP is suspended 150 m above the seafloor, Equation B.2 gives:

$$P = \rho ghQ = 1302.4 \text{ kg/m}^3 \times 10 \text{ m/s}^2 \times 150 \text{ m} \times 0.186 \text{ m}^3/\text{s} = 363.37 \text{ kW}$$

As the inner riser diameter of the rigid steel pipe of the Solwara 1 UTS is 12 1/8 inches (approx. 308 mm) and the riser transfer pipe of the CM is 10 inches (approx. 254 mm) an increase in the required power to lift the slurry at the same flow rate is reasonable to assume, the increase is estimated to be 20%. In addition to this, assuming the same efficiency of $\approx 80.0\%$ for the SPT pump system as the UTS the required power is even higher.

Another factor of the SPT pump system is that according to [10] the SSLP requires an input pressure of 5 bar as the PD-pump system does not provide any suction. This additional requirement is fulfilled by adding 0.5 MPa (= 5 bar) to the ρgh of Equation B.2.

By adding all this correction factors to Equation B.2 the following is obtained:

$$P = (\rho gh + 0.5 \text{ MPa})Q \times 1.25 \times 1.25 = 684.55 \text{ kW}$$

This estimation is based on a series of simplifications. In addition to the above factors an additional correction factor between 10-30% is added to the AUX, BM and CM pump systems. Although the many simplifications and assumptions the values, in the range of 750-900 kW, of the SPT installed pump effect is considered to be reasonable.

Appendix C

DSM System Topologies

C.1 Nautilus Minerals' SPS

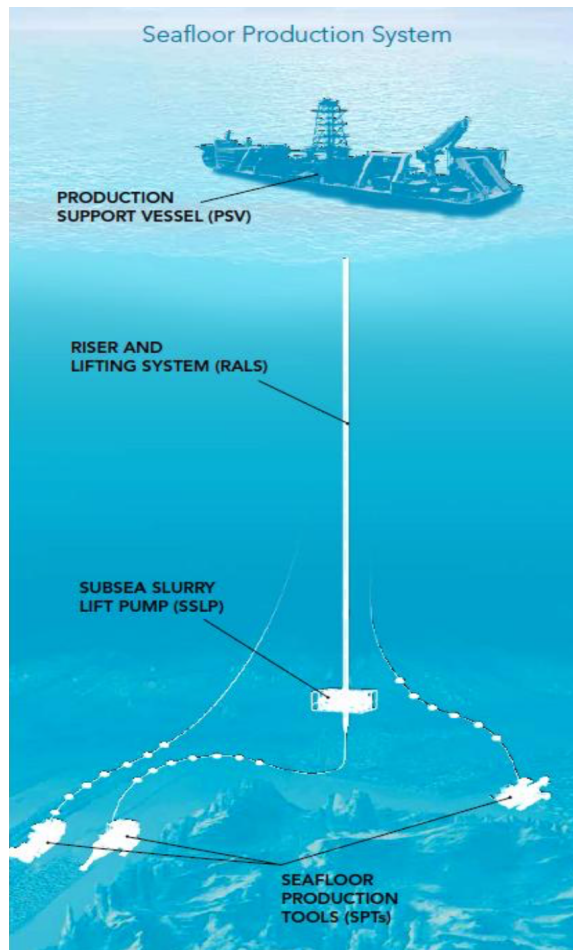


Figure C.1: Nautilus Minerals SPS [46, p. 12].

C.2 BAUER and Technip Vertical Miner

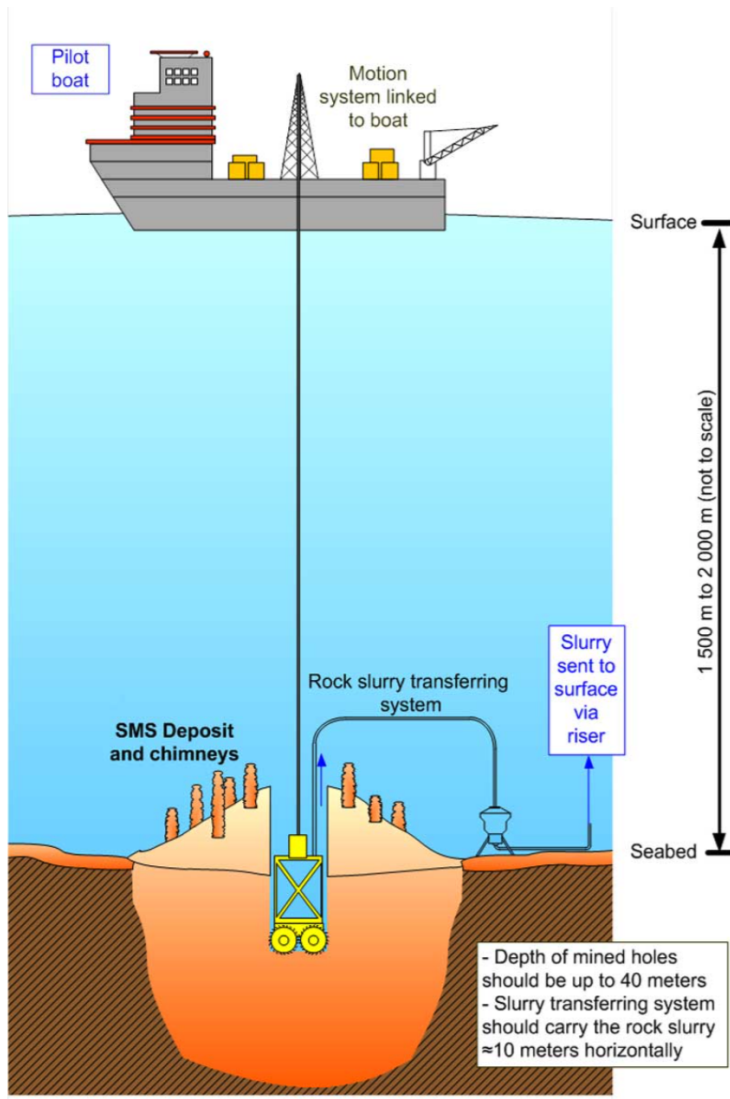


Figure C.2: BAUER and Technip Vertical Miner [8, Fig. 2].

Appendix D

Single Line Diagrams

D.1 Symbols

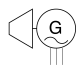

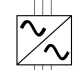
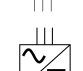
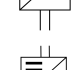
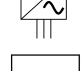


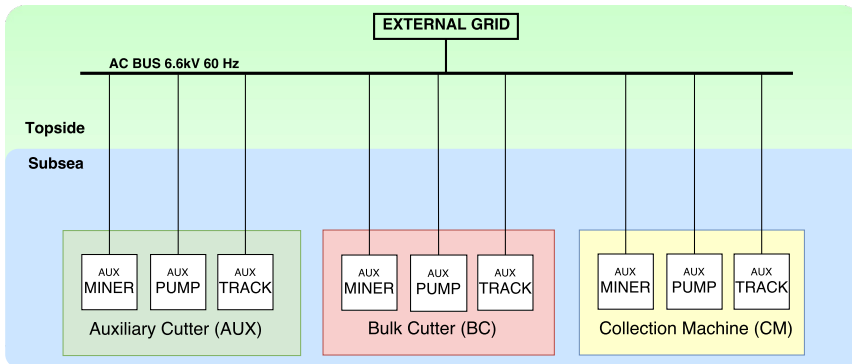
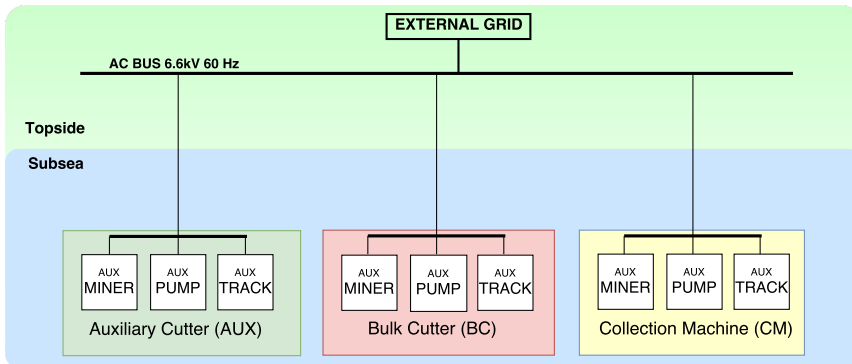
	Turbine-Generator Set
	SSLP Pump Motor
	AC/AC converter (frequency converter)
	AC/DC converter (rectifier)
	DC/AC converter (inverter)
	Passive Load
	Mining Tool Motor
	Centrifugal Pump Motor

Table D.1: Explanation of SLD Symbols.

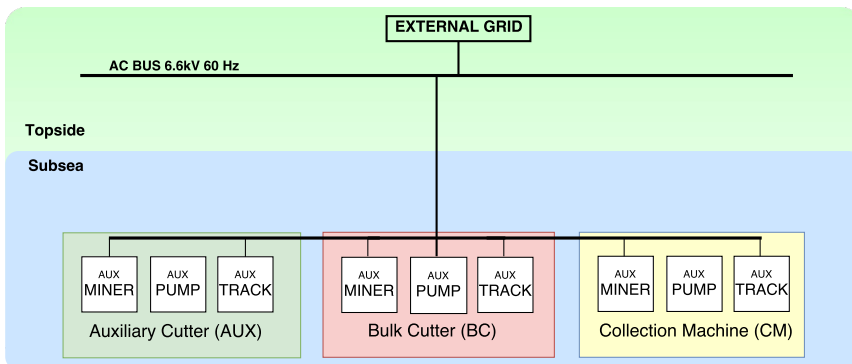
D.2 Simple Models



(a) SLD Model A.



(b) SLD Model B.



(c) SLD Model C.

Figure D.1: Model A, B and C SLD.

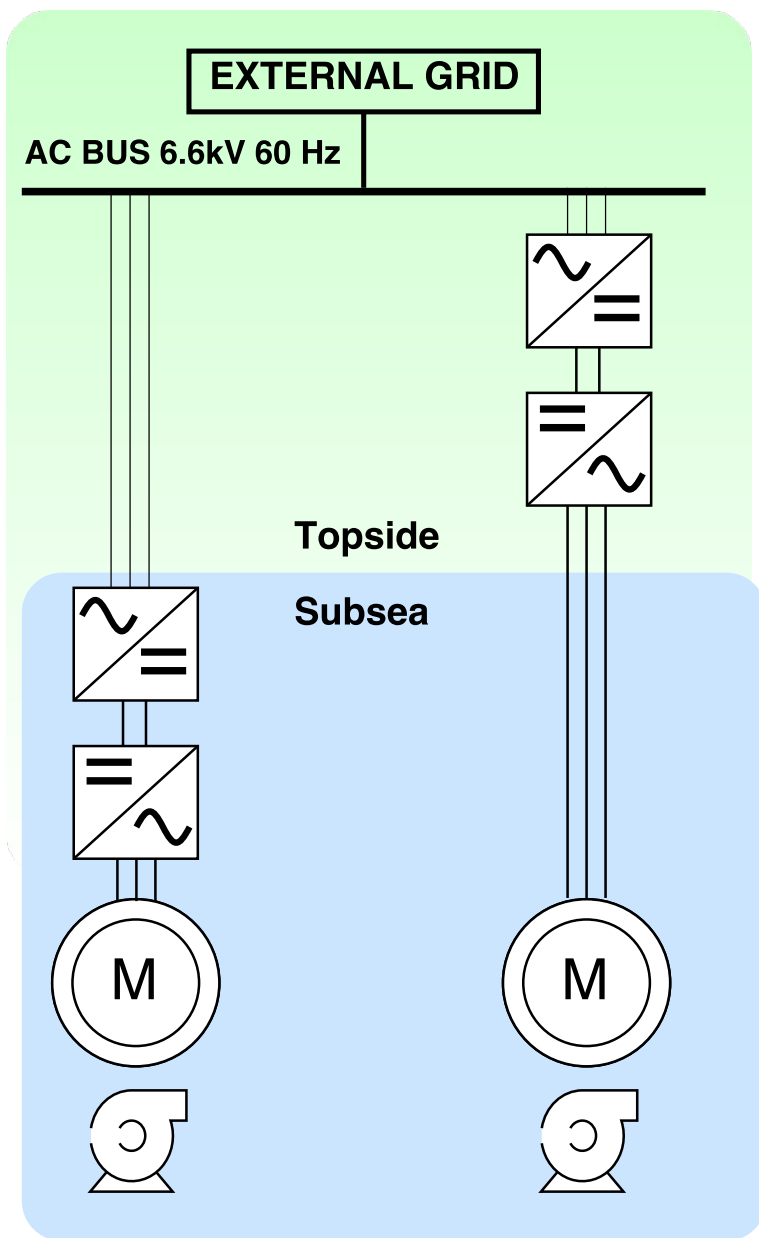


Figure D.2: Model D SLD.

Appendix E

Model A, B and C Load Flow Simulation Results

SPT	Component	Model A			Model B		
		Cable (XLPE-CU)		V_d	Cable (XLPE-CU)		V_d
		Size	Loading	[%]	Size	Loading	[%]
AUX	Pump	3×25 mm	60.60 %	6	3×185 mm	60.63 %	4
	Tool	3×25 mm	60.60 %	6			
	Track	3×25 mm	68.80 %	7			
BC	Pump	3×25 mm	60.60 %	6	3×240 mm	70.73 %	4
	Tool	3×50 mm	69.26 %	6			
	Track	3×35 mm	71.17 %	6			
CM	Pump	3×25 mm	68.80 %	7	3×150 mm	62.78 %	4
	Tool	3×25 mm	36.91 %	4			
	Track	3×25 mm	60.60 %	6			

Table E.1: Model A and Model B load flow simulation cable size, loading and voltage drop.

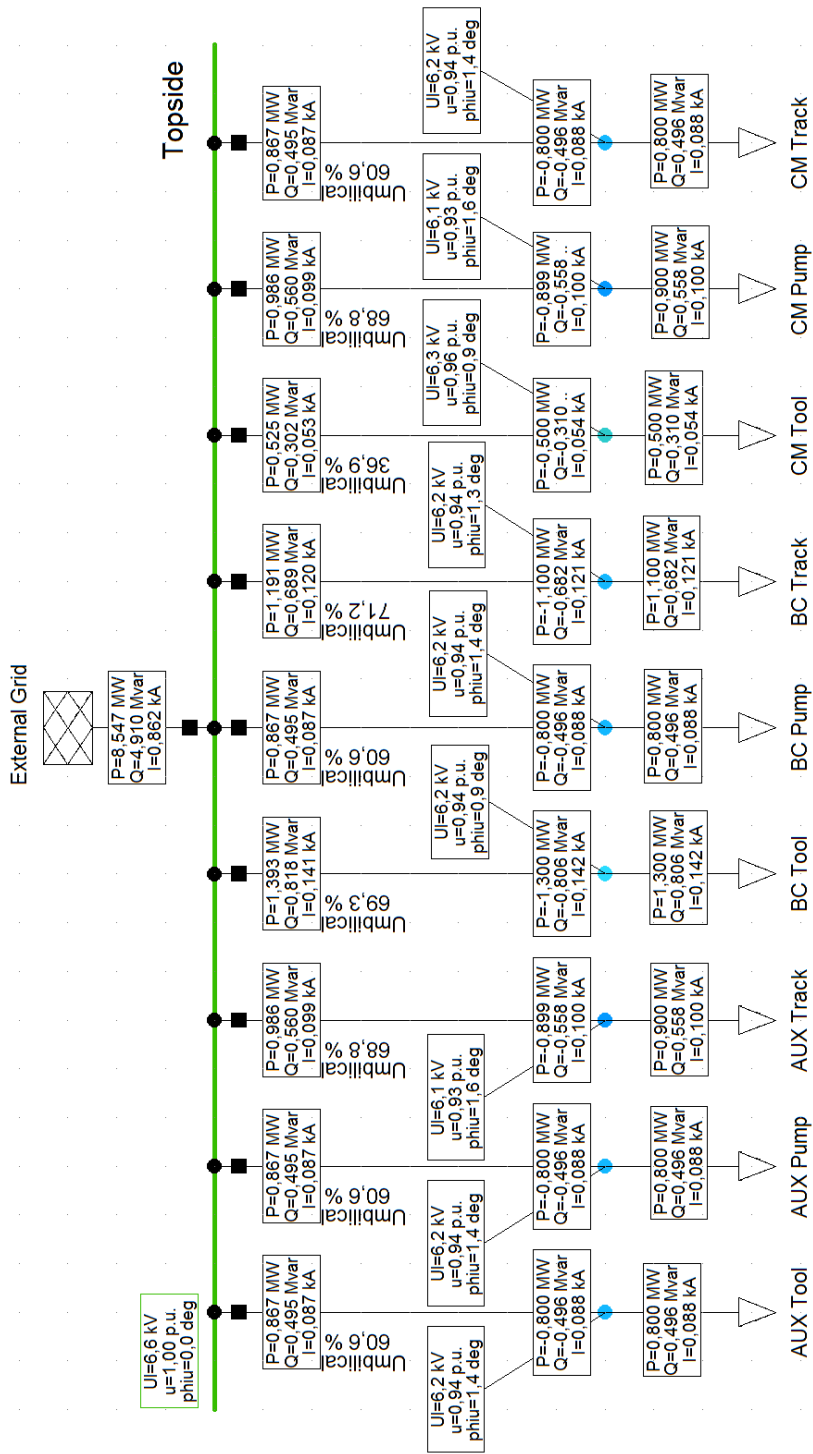


Figure E.1: Load Flow Model A.

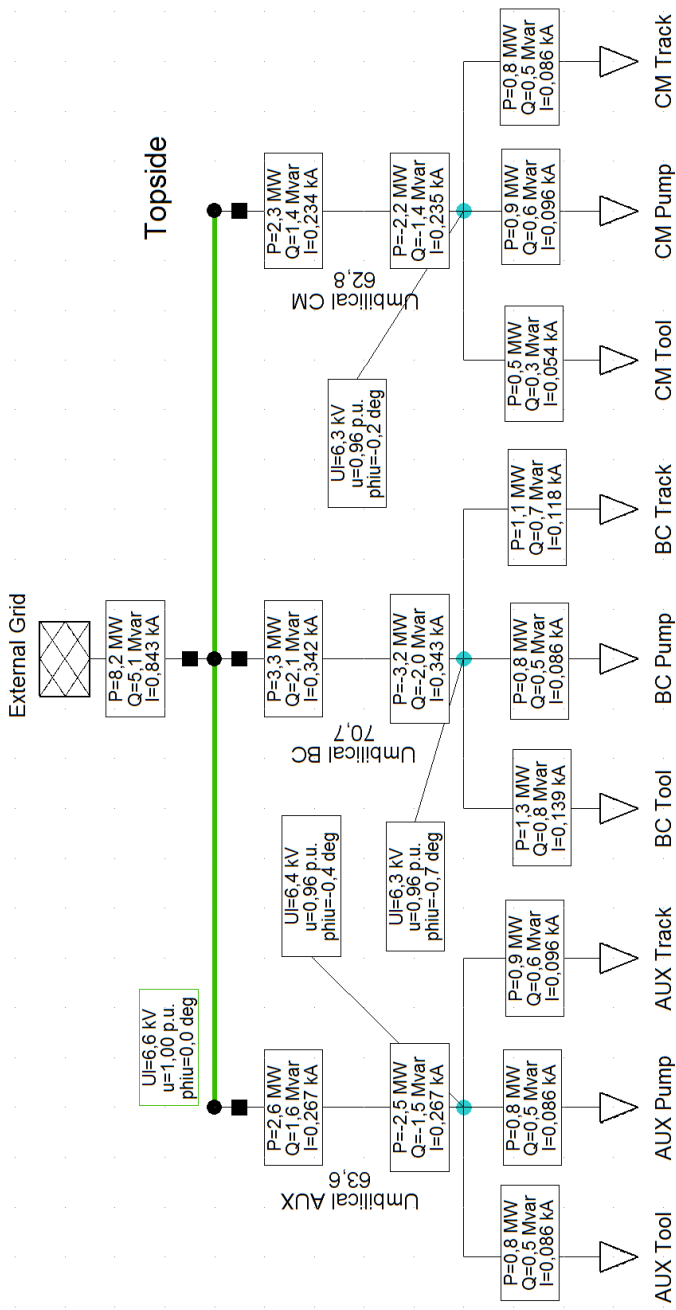


Figure E.2: Load Flow Model B.

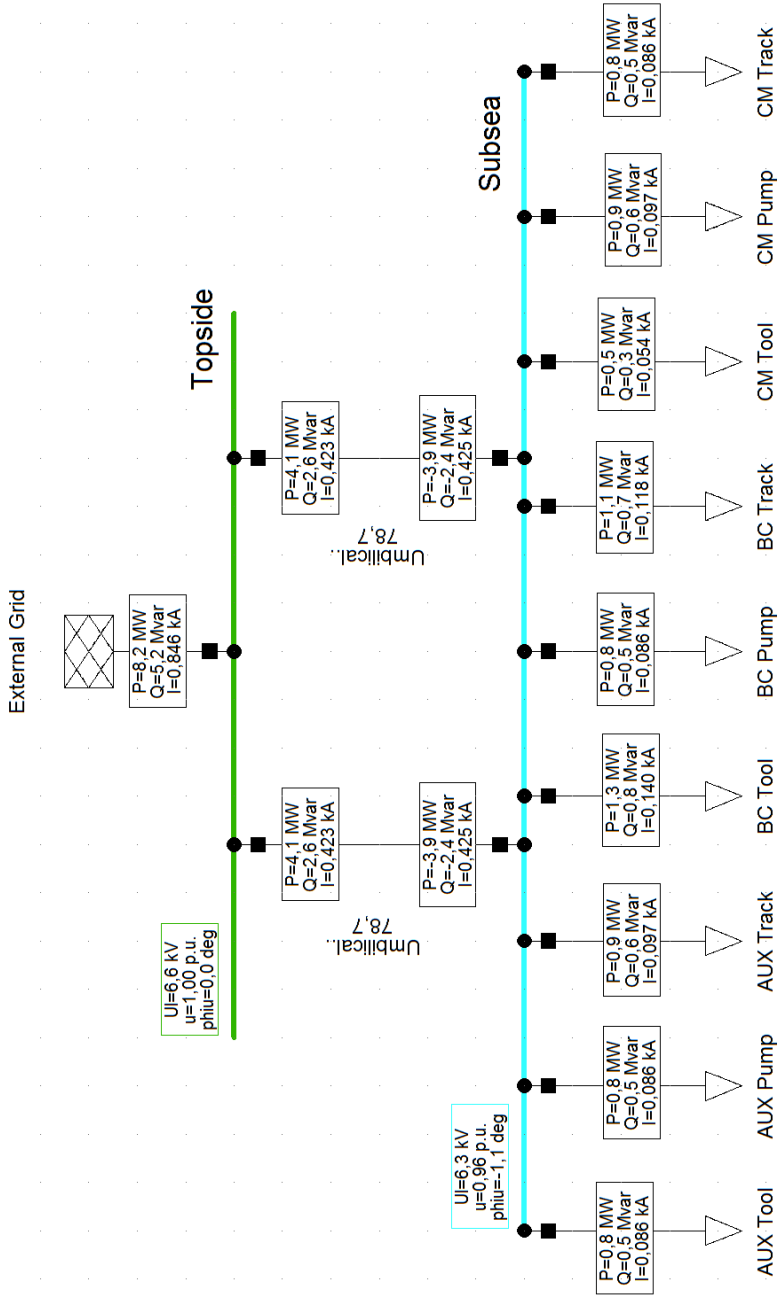


Figure E.3: Load Flow Model C.

Appendix F

Model 1, 2, 3 and 4 Load Flow Simulation Results

		Model 1	Model 2
Generation	Installed Capacity	28.90 MW	28.90 MW
	Spinning Reserve	3.42 MW	3.47 MW
	Active Power	25.48 MW	25.43 MW
	Reactive Power	12.35 MVA _r	12.53 MVA _r
	Apparent Power	28.32 MVA	28.35 MVA
Passive Load	Active Power	11.60 MW	11.60 MW
	Reactive Power	8.71 MVA _r	8.85 MVA _r
	Apparent Power	14.51 MVA	14.59 MVA
Motor Load	Active Power	13.65 MW	13.65 MW
	Reactive Power	5.63 MVA _r	5.63 MVA _r
	Apparent Power	14.77 MVA	14.77 MVA
Grid Losses	Active Power	0.23 MW	0.18 MW
	Reactive Power	0.07 MVA _r	0.11 MVA _r
Line Charging	Reactive Power	-0.06 MVA _r	-0.05 MVA _r
Total P.F.	Generation	0.90	0.90
	Passive Load	0.80	0.80
	Motor	0.92	0.92

Table F.1: Model 1 and 2: Load flow simulation results.

		Model 3	Model 4
Generation	Installed Capacity	28.90 MW	28.90 MW
	Spinning Reserve	3.42 MW	3.54 MW
	Active Power	25.48 MW	25.36 MW
	Reactive Power	10.40 MVA _r	10.40 MVA _r
	Apparent Power	27.52 MVA	27.52 MVA
Passive Load	Active Power	11.60 MW	11.60 MW
	Reactive Power	6.82 MVA _r	6.82 MVA _r
	Apparent Power	13.46 MVA	13.46 MVA
Motor Load	Active Power	13.65 MW	13.65 MW
	Reactive Power	5.63 MVA _r	5.63 MVA _r
	Apparent Power	14.77 MVA	14.77 MVA
Grid Losses	Active Power	0.23 MW	0.11 MW
	Reactive Power	0.01 MVA _r	0.02 MVA _r
Line Charging	Reactive Power	0.00 MVA _r	0.00 MVA _r
Total P.F.	Generation	0.93	0.93
	Passive Load	0.86	0.86
	Motor	0.92	0.92

Table F.2: Model 3 and 4: Load flow simulation results.

Appendix G

Cable Data

Type Cross section		XLPE-CU			
		$3 \times 70 \text{ mm}^2$	$3 \times 95 \text{ mm}^2$	$3 \times 120 \text{ mm}^2$	$3 \times 185 \text{ mm}^2$
V_{rated}	kV	11.0	11.0	11.0	11.0
I_{rated}	A	245	295	335	420
R'	Ω/km	0.268	0.193	0.153	0.099
X'	Ω/km	0.106	0.100	0.097	0.092
L'	mH/km	0.337	0.318	0.309	0.293
C'	$\mu\text{F}/\text{km}$	0.318	0.360	0.392	0.510

Table G.1: Technical data of the cables selected for AC distribution.

Type Cross-section		N1YSY			
		$1 \times 120 \text{ mm}^2$	$1 \times 150 \text{ mm}^2$	$1 \times 300 \text{ mm}^2$	$1 \times 500 \text{ mm}^2$
V_{rated}	kV	10.0	10.0	10.0	10.0
I_{rated}	A	375	410	575	682
R'	Ω/km	0.156	0.128	0.065	0.037
X'	Ω/km	0.113	0.110	0.101	0.085
L	mH/km	0.360	0.350	0.32	0.271
C'	$\mu\text{F}/\text{km}$	0.350	0.380	0.500	0.61

Table G.2: Technical data of the cables selected for DC distributions.

Cable Parameters:

V_{rated} Rated Voltage
 I_{rated} Rated Current

per Length 1,2-Sequence:

R' AC-Resistance (20°C)
 X' Reactance
 L' Inductance
 C' Capacitance



Norwegian University of
Science and Technology

Norwegian University of Science and Technology
Department of Electric Power Engineering
Trondheim